SANDIA REPORT

SAND2015-8380
Unlimited Release
September 2015

Dynamic High-Temperature Characterization of an Iridium Alloy in Tension

Bo Song, Kevin Nelson, Helena Jin, Ronald Lipinski, John Bignell,
Sandia National Laboratories

G. B. Ulrich
Oak Ridge National Laboratory

E. P. George
Ruhr University Bochum

Prepared by
Sandia National Laboratories
Albuquerque, New Mexico 87185 and Livermore, California 94550

Sandia National Laboratories is a multi-program laboratory managed and operated by Sandia Corporation, a wholly owned subsidiary of Lockheed Martin Corporation, for the U.S. Department of Energy's National Nuclear Security Administration under contract DE-AC04-94AL85000.

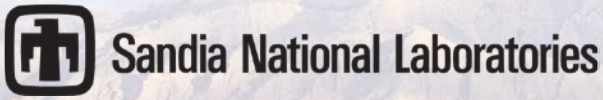

Issued by Sandia National Laboratories, operated for the United States Department of Energy by Sandia Corporation.

Available to DOE and DOE contractors from
U.S. Department of Energy
Office of Scientific and Technical Information
P.O. Box 62
Oak Ridge, TN 37831

Telephone: (865) 576-8401
Facsimile: (865) 576-5728
E-Mail: reports@adonis.osti.gov
Online ordering: http://www.osti.gov/bridge

Available to the public from
U.S. Department of Commerce
National Technical Information Service
5285 Port Royal Rd.
Springfield, VA 22161

Telephone: (800) 553-6847
Facsimile: (703) 605-6900
E-Mail: orders@ntis.fedworld.gov
Online order: http://www.ntis.gov/help/ordermethods.asp?loc=7-4-0#online

SAND2015-8380
Unlimited Release
September 2015

Dynamic High-Temperature Characterization of an Iridium Alloy in Tension

Bo Song[1], Kevin Nelson[2], Helena Jin[2], Ronald Lipinski[3], John Bignell[4],
[1] Experimental Environment Simulation Department; [3] Advanced Nuclear Fuel Cycle Technology Department; [4] Structural and Thermal Analysis Department
Sandia National Laboratories
P.O. Box 5800, Albuquerque, New Mexico 87185
[2] Mechanics of Materials Department
Sandia National Laboratories
P.O. Box 0969, Livermore, California 94550

G. B. Ulrich
Radioisotope Power Systems Program
Oak Ridge National Laboratory
Oak Ridge, Tennessee 37831-6079

E. P. George
Institute for Materials
Ruhr University Bochum
Universitaetstr. 150
44801 Bochum, Germany

Abstract

Iridium alloys have been utilized as structural materials for certain high-temperature applications, due to their superior strength and ductility at elevated temperatures. The mechanical properties, including failure response at high strain rates and elevated temperatures of the iridium alloys need to be characterized to better understand high-speed impacts at elevated temperatures. A DOP-26 iridium alloy has been dynamically characterized in compression at elevated temperatures with high-temperature Kolsky compression bar techniques. However, the dynamic high-temperature compression tests were not able to provide sufficient dynamic high-temperature failure information of the iridium alloy. In this study, we modified current room-temperature Kolsky tension bar techniques for obtaining dynamic tensile stress-strain curves of the DOP-26 iridium alloy at two different strain rates (~1000 and ~3000 s^{-1}) and temperatures (~750°C and ~1030°C). The effects of strain rate and temperature on the tensile stress-strain response of the iridium alloy were determined. The DOP-26 iridium alloy exhibited high ductility in stress-strain response that strongly depended on both strain rate and temperature.

ACKNOWLEDGMENTS

The authors would like to acknowledge Kevin Connelly for his initial specimen and fixture design support to this project.

This work was sponsored by the United States Department of Energy (DOE) Office of Space and Defense Power Systems (NE-75). The authors gratefully acknowledge the support and guidance of Ryan D. Bechtel of the U.S. Department of Energy.

Sandia National Laboratories is a multi-program laboratory managed and operated by Sandia Corporation, a wholly owned subsidiary of Lockheed Martin Corporation, for the U.S. Department of Energy's National Nuclear Security Administration under contract DE-AC04-94AL85000.

Oak Ridge National Laboratory is a multi-program research laboratory managed by UT-Battelle, LLC, for the U.S. DOE under contract DE-AC05-00OR22725.

CONTENTS

FIGURES

TABLES

NOMENCLATURE

CCT	Cold contact time
DIC	Digital image correlation
EDM	Electrical discharge machining
SEG	Super enhanced graphite
SHB	Split Hopkinson bar
SNL	Sandia National Laboratories
ORNL	Oak Ridge National Laboratory

This page intentionally left blank.

1. INTRODUCTION

Iridium alloys possess unique combinations of high melting temperature, high-temperature strength and ductility, and excellent oxidation and corrosion resistance [1], making them ideal for high-temperature applications. In some applications, the high-temperature high-strain-rate mechanical response, including failure response, of the materials must be understood in order to meet the safety requirement for the design of components. Dynamic high-temperature stress-strain data are thus needed to develop strain-rate and temperature dependent material models for safety analysis. However, the mechanical stress-strain data of iridium alloys at high strain rates and elevated temperatures has been very limited in the literature [2-6].

Kolsky bar (also called split Hopkinson bar, SHB) testing has been recognized as an effective and efficient tool to characterize the stress-strain response of materials at high strain rates between 10^{-2} and 10^{4} s^{-1}. However, it has been challenging to dynamically characterize materials at high temperatures, particularly when the temperature is higher than 600°C [7]. Recently, Song et al. [8, 9] modified Kolsky compression bar techniques to characterize the dynamic stress-strain properties of a DOP-26 iridium alloy in compression at high strain rates (300 - 10000 s^{-1}) and high temperatures (750 and 1030°C). The iridium alloy showed significant strain-rate and temperature effects on the compressive stress-strain response. However, the dynamic compression tests were not capable of providing sufficient ductility and/or failure information of the iridium alloy at high strain rates and temperatures. Therefore, dynamic tensile stress-strain characterization of the iridium alloy at high temperatures is recommended.

The Kolsky bar technique was originally developed for dynamic compression tests by Kolsky in 1949 [10]. Based on the same principles, the first Kolsky tension bar was developed by Harding in 1960 [11] and a variety of Kolsky tension bars have been developed since then. The most commonly used method is direct-tension Kolsky bars [12-14]. For example, Song et al. [14] launched a solid striker to an end cap on the open end of the gun barrel to generate a dynamic tensile load in the bar system. The schematic and design of the Kolsky tension bar are shown in Fig. 1. Figure 2 shows an actual photograph of the Kolsky tension bar. Both incident and transmission bars were made of C350 maraging steel and had a common diameter of 19.05 mm. One end of the incident bar was attached to the steel gun barrel, which had an OD of 31.8 mm and ID of 19.05 mm, through a coupler. The other end of the incident bar was attached to the specimen with an adapter. The specimen was attached to the transmission bar end in the same manner. The specimen ends of both the incident and transmission bars had ½"-20 female threads. One end of the adapter had ½"-20 male threads, whereas the other end was specially designed for specimen installation, depending on the material under investigation. The gun barrel was covered with a threaded end cap. A 19.05 mm diameter solid striker was placed in the gun barrel and propelled by compressed air through a flexible tube with a poppet valve, as shown in Fig. 1(b). As indicated in Fig. 1(b), the gun barrel and the incident bar were 1828.8 and 3657.6 mm long, respectively. The transmission bar was 2133.6 mm long. The length of the striker can be varied depending on the total loading duration required. The air pressure that is suddenly released by the poppet valve pushes the striker forward until it impacts the end cap, generating a dynamic tensile loading in the gun barrel. The tensile stress wave in the gun barrel is then transmitted into

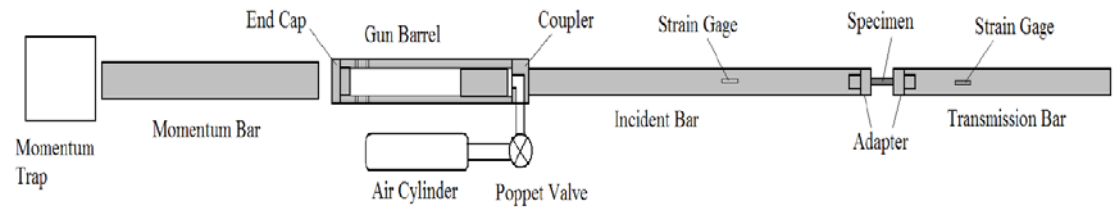

(a)

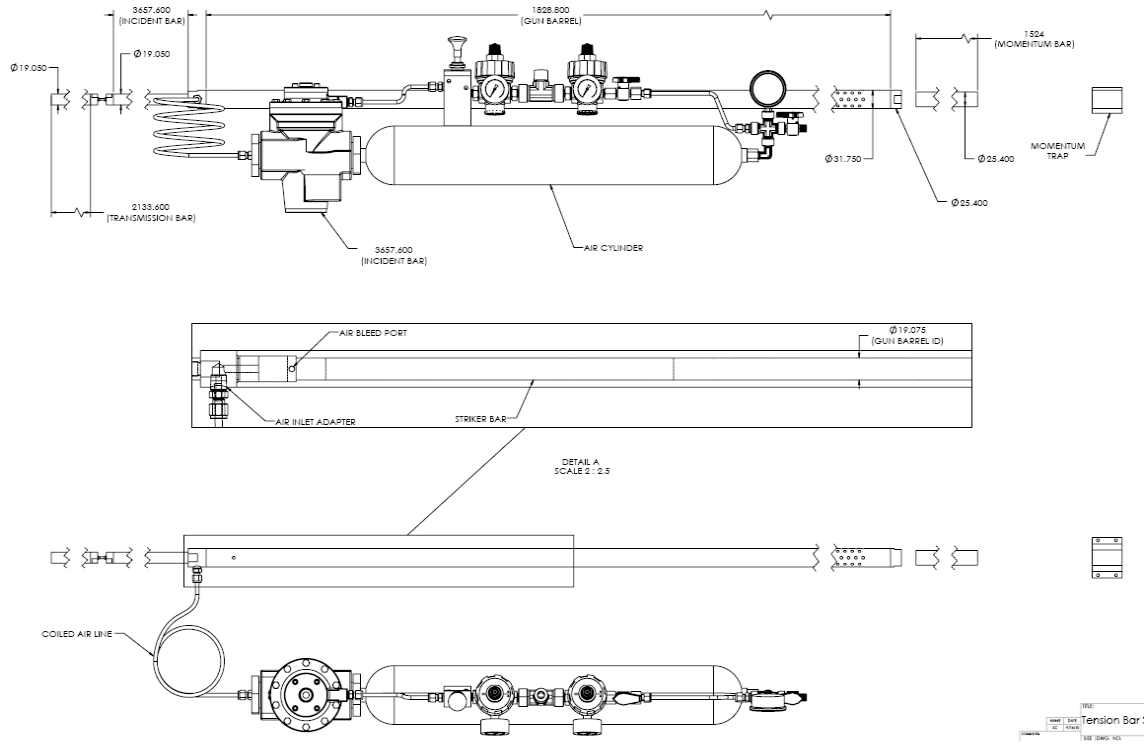

Unit: mm

(b)

Figure 1. Conventional Kolsky tension bar system.

Figure 2. Photograph of the Kolsky tension bar system.

the attached incident bar, which is recorded as an "incident wave" with the strain gages on the incident bar. When the incident wave arrives at the incident bar/specimen interface, part of it is reflected back into the incident bar as a "reflected wave" recorded with the same strain gages and the balance is transmitted into the transmission bar through the specimen as a "transmitted wave" that is recorded with the strain gages on the transmission bar (Fig. 1(a)). Both the incident and transmission bars are slender to ensure nearly one-dimensional stress wave propagation. According to one-dimensional stress wave theory, the strain rate ($\dot{\varepsilon}$), strain (ε), and stress (σ) in the specimen are calculated as [7]

$$\dot{\varepsilon} = \frac{V_1 - V_2}{L_s} = \frac{C_B}{L_s}\left(\varepsilon_i - \varepsilon_r - \varepsilon_t\right) \tag{1}$$

$$\varepsilon = \int_0^t \dot{\varepsilon} dt = \frac{C_B}{L_s}\int_0^t \left(\varepsilon_i - \varepsilon_r - \varepsilon_t\right) dt \tag{2}$$

$$\sigma_1 = \frac{A_B}{A_s} \cdot E_B\left(\varepsilon_i + \varepsilon_r\right) \tag{3}$$

$$\sigma_2 = \frac{A_B}{A_s} \cdot E_B \varepsilon_t \tag{4}$$

where the subscripts, i, r, and t, represent the incident, reflected, and transmitted pulses, respectively; V_1 and V_2 are the velocities of the front and back ends of the specimen, respectively; L_s is the original length of the specimen; A_B and A_s are the cross-sectional areas of the bars and the gage section of the specimen, respectively; C_B and E_B are one-dimensional elastic longitudinal wave speed and Young's modulus of the bar material, respectively; σ_1 and

σ_2 represent the stresses at the front and back ends of the specimen, respectively. When the specimen stress is equilibrated,

$$\sigma_1 = \sigma_2 \tag{5a}$$

or

$$\varepsilon_i + \varepsilon_r = \varepsilon_t \tag{5b}$$

the calculations of specimen strain rate, strain, and stress are then simplified as

$$\dot{\varepsilon} = -2\frac{C_B}{L_S}\varepsilon_r \tag{6}$$

$$\varepsilon = -2\frac{C_B}{L_S}\int_0^t \varepsilon_r dt \tag{7}$$

$$\sigma = \frac{A_B}{A_s}\cdot E_B \cdot \varepsilon_t \tag{8}$$

The stress-strain curve can be obtained by eliminating the term of time in Eqs. (7) and (8).

Unlike in Kolsky compression bar tests, the specimen in Kolsky tension bar tests needs to be firmly attached to the ends of the incident and transmission bars. Cylindrical tensile specimens can be directly threaded into the bar ends. However, when the Kolsky tension bar is used to characterize sheet metals, i.e., the iridium alloy in this study, special fixtures need to be carefully designed to attach the specimen to the bar ends. The uncertainties in the resultant stress-strain measurements of the specimen become more significant when the complexity of the fixtures increases. For example, the addition of the fixtures may produce very complicated interfaces between the bar ends and the tensile specimen, which may modify the stress wave propagation. In this case, the reflected wave in Eqs. (6) and (7) may not be appropriate to calculate the strain rate and strain histories in the specimen. Alternative methods that use non-contact optical techniques to measure the specimen strain and strain rate are therefore needed.

Use of laser “extensometry” has become a straight forward non-contact method to measure specimen strain in Kolsky bar experiments. In this technique (which will be described in a subsequent section), a uniform laser sheet is generated to cover the entire gage section of the specimen. When the specimen deforms, a change in the gage length of the specimen results in a change in the pass-through light intensity that is collected by a high-frequency-response laser detector [15, 16]. Through proper calibration, the temporal history of the gage length of the deforming specimen can be measured to calculate the corresponding strain history in the specimen. Satisfactory results were reported on using this technique to measure the dynamic tensile behavior of different materials with a Kolsky tension bar system [17-19]. In a typical Kolsky bar experiment, both the incident and transmission bar ends move in the same direction

but at different velocities. A rigid body motion may be superimposed to the absolute deformation of the specimen. If there is a slight variation in laser intensity along the measurement gage section (which is often the case in experimental practice), the rigid body motion will induce a small output signal obscuring the actual specimen deformation particularly at small strains. In order to demonstrate the variation in the laser intensity, the local laser sensitivities were carefully calibrated over a small range (~200 μm) at three adjacent locations approximately 300 μm apart. In each calibration, a high-resolution differential translation stage was applied to generate a gap size increment of 10-μm.

Figure 3 summarizes the calibration results in terms of the gap size versus laser detector voltage output. The relationship between the two parameters exhibits a reasonable linearity at all three locations but with slightly different slopes due to the variation in local laser intensity. This difference in slope at different locations indicates different sensitivities of the laser system, which may generates significant errors in specimen strain measurements, particularly when the specimen strains are small. In addition to the error caused by the rigid body motion, the measurement resolutions in current laser extensometer techniques are limited particularly at small strains due to the relatively long gage section in Kolsky tension bar experiments. Using a laser system to track the displacement at the incident bar/specimen interface has been only recently proposed to improve the resolution [20]. However, the 100-μm resolution of the laser detector used in [20] was still insufficient for obtaining reliable stress-strain responses of the material under investigation at small strains.

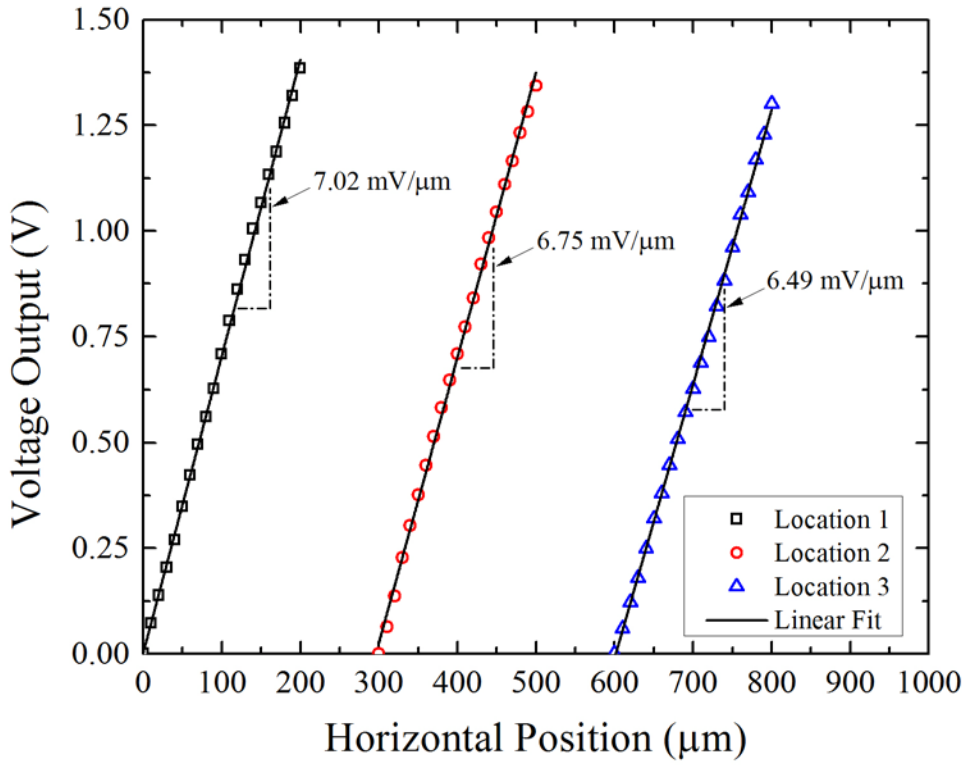

Figure 3. Conventional laser calibrations at different locations.

Digital image correlation (DIC) is another non-contact technique that has been improved and extended to Kolsky bar experiments for dynamic full-field strain measurements in the specimen [21-23]. However, the resolution of the high-rate DIC highly depends on the frame rate, maximum number of frames, and image resolution of the camera, in addition to a number of other challenges including reliable patterning and proper lighting on the specimen surface. The high-rate DIC provides valuable information on the uniformity of deformation in the specimen during dynamic loading but insufficient data points and/or image resolution to construct a precise stress-strain curve due to the extreme difficulty in acquiring a large quantity of high-resolution images at very high frame rates [20].

In addition to the diagnostic issues in Kolsky tension bar experiments presented above, it is even more challenging when the Kolsky tension bar is used for high-temperature experiments. The concepts for high-temperature Kolsky compression bar techniques developed previously [7, 8] cannot be used for high-temperature Kolsky tension bar tests. In previous high-temperature Kolsky compression bar experiments, the specimen was individually heated to high temperatures while the pressure bars were kept at room temperature. The hot specimen was then quickly placed between the incident and transmission bars right before dynamic loading. This procedure was precisely controlled to minimize the cold contact time (CCT) between the "hot" specimen and the "cold" pressure bars. Even though different methods have been developed to shorten the CCT, they cannot be applied to high-temperature Kolsky tension bar testing because the tensile specimen must be installed to the bar ends before heating. In this case, the heat will transfer from the "hot" specimen to the room-temperature bars, resulting in a temperature drop in the tensile specimen and a temperature gradient in the bars before dynamic loading. Su et al. [24] applied thermal-protective coating with a very low heat transfer coefficient to the bar surface to mitigate the heat transfer to the bars. Using the same method, the temperature in the bars was reduced to below 300°C when the specimen was heated to 527°C by Guo and Gao [25]. The heat was still transferred from the high-temperature specimen to the bars through the threads, which consequently generated a thermal gradient in the bars. Such a thermal gradient may become more significant when the testing temperature increases. A significant thermal gradient will result in erroneous stress and strain measurements in the specimen. These challenges limit current Kolsky tension bar tests to temperatures below 600°C [24-28]. Thus, special experimental design considerations are required for Kolsky tension bar experiments at higher temperatures, i.e., 750 and 1030°C in this study.

Additional challenges are encountered when using Kolsky tension bar techniques for dynamic high-temperature characterization. For example, when the specimen is heated to high temperatures (~750 and 1030°C in this study), the thermal-expansion of the specimen must be considered and addressed. Also, significant thermal-softening of the specimen materials at high temperatures results in a very weak transmitted signal which, nevertheless, must be measured with reasonably high resolution.

In this study, the conventional Kolsky tension bar was modified, through proper designs in experimental setup, fixtures and specimen, as well as electrical and optical diagnostics, to characterize the dynamic tensile stress-strain response of a thin-sheet DOP-26 iridium alloy at elevated temperatures. The DOP-26 iridium alloy was characterized at two different strain rates

(~1000 and ~3000 s^{-1}) and temperatures (~750 and ~1030°C) in order to determine the effects of strain rate and temperature on the tensile stress-strain response.

This page intentionally left blank.

2. HIGH-TEMPERATURE KOLSKY TENSION BAR FOR THIN IRIDIUM SPECIMEN CHARACTERIZATION

In this section, the high-temperature Kolsky tension bar technique is presented along with the issues encountered and associated measurement techniques for dynamic high-temperature tensile characterization of the DOP-26 iridium alloy.

2.1. The High-temperature Kolsky Tension Bar at SNL

In this study, the room-temperature Kolsky tension bar shown in Figs. 1 and 2 was modified for dynamic high-temperature characterization of the DOP-26 iridium alloy. Figure 4 shows a schematic of the modified high-temperature Kolsky tension bar system. The detailed modifications are shown in Fig. 5. Since it is not possible to directly thread a thin and flat iridium specimen into the bar ends, a pair of specimen fixtures was designed, as shown in Fig. 5(a). The thin-sheet specimen was made into a dog-bone shape. The fixtures were machined with a slot with the same dimensions as the non-gage section of the specimen such that the whole non-gage section of the specimen was placed into the slot of the fixture. The specimen was then covered with a semicircular cap. The depth of the fixture was made the same as the specimen thickness such that the semicircular cap did not provide additional normal force on the specimen but retained the specimen during dynamic loading. Both the fixtures and the semicircular caps were made of Inconel 718 steel, which can maintain relatively high strength at elevated temperatures.

An induction coil heater was installed on the testing section. Due to the small size of the specimen under investigation, the induction coil was set to heat the relatively large fixtures and then let the heat transfer to the specimen (Fig. 5(b)). This experimental design also enables direct measurement of displacements at the specimen ends using a laser extensometer. When the fixtures are heated with the induction coil, the heat is transferred to both the specimen and the bars simultaneously. In order to prevent heating of the bars, a pair of hollow water-cooled pillow blocks was installed on the bar ends, as shown in Fig. 5(c). This design is similar in principle to that developed by Scapin et al. [29]. The difference is that Scapin et al. [29] applied a Cortex-tube-based air cooling system to cool down the bars for testing up to 400°C. As shown in Fig. 5(c), the same Frelon® coated linear bearing was placed in the center of the pillow block to support the bars and the testing fixture with minimal friction in between. The O rings on the linear bearing were removed and additional thermal-conductive grease was applied between the linear bearings and the pillow blocks to increase thermal conductivity from the pillow block to the bars. The water cooling system used in this study was shown to be capable of cooling the bars at or even below room temperature when the testing temperature was as high as 1030°C.

When the thin iridium specimen is heated, i.e. to 750 and 1030°C in this study, the specimen may become longer due to thermal expansion. However, the force generated by such a thermal expansion may not be sufficiently high to overcome the friction between the bars and the bar supports and to push the incident and transmission bars back. As a consequence, the thin iridium specimen may buckle. The buckling generated in the specimen will produce an erroneous stress-strain response which is difficult to correct. A spring-loaded pre-tension system, as shown in Fig.

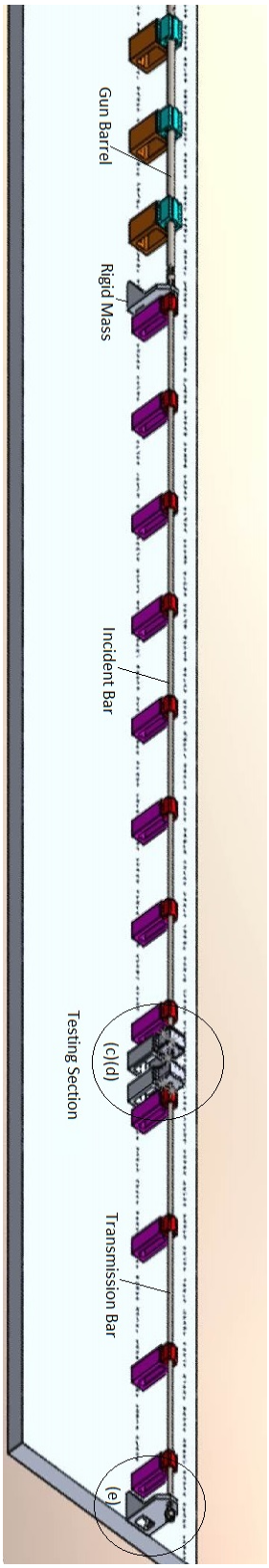

Figure 4. Schematic of high-temperature Kolsky tension bar system.

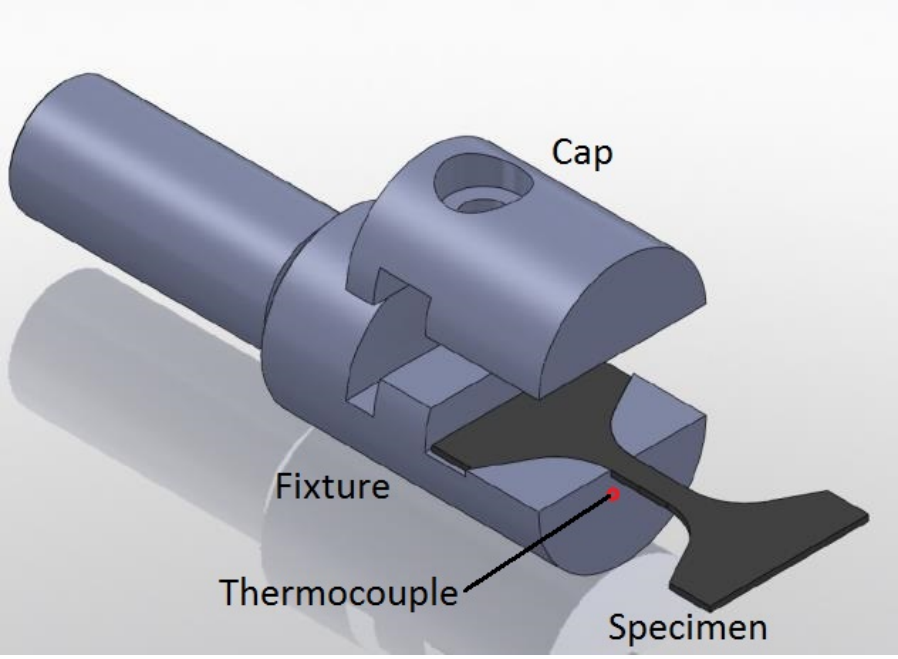

(a)

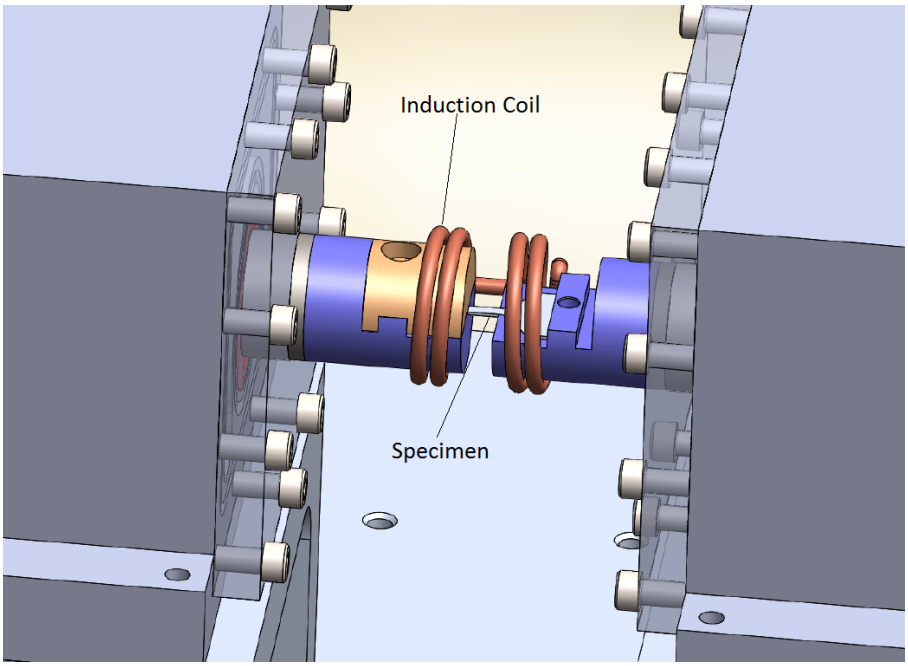

(b)

Figure 5. Modifications to Kolsky tension bar for high-temperature testing. a) specimen and fixture design; b) induction heater

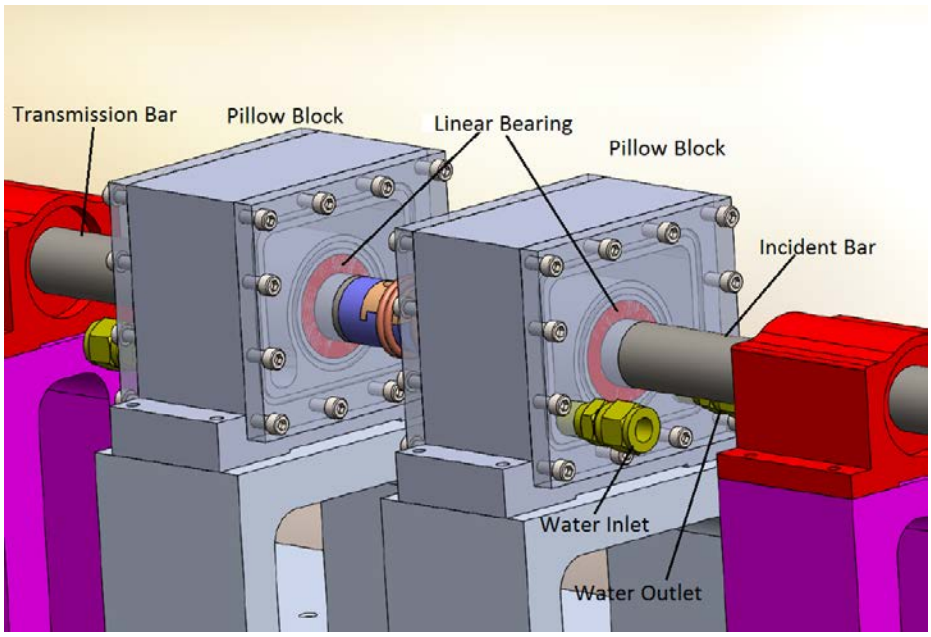

(c)

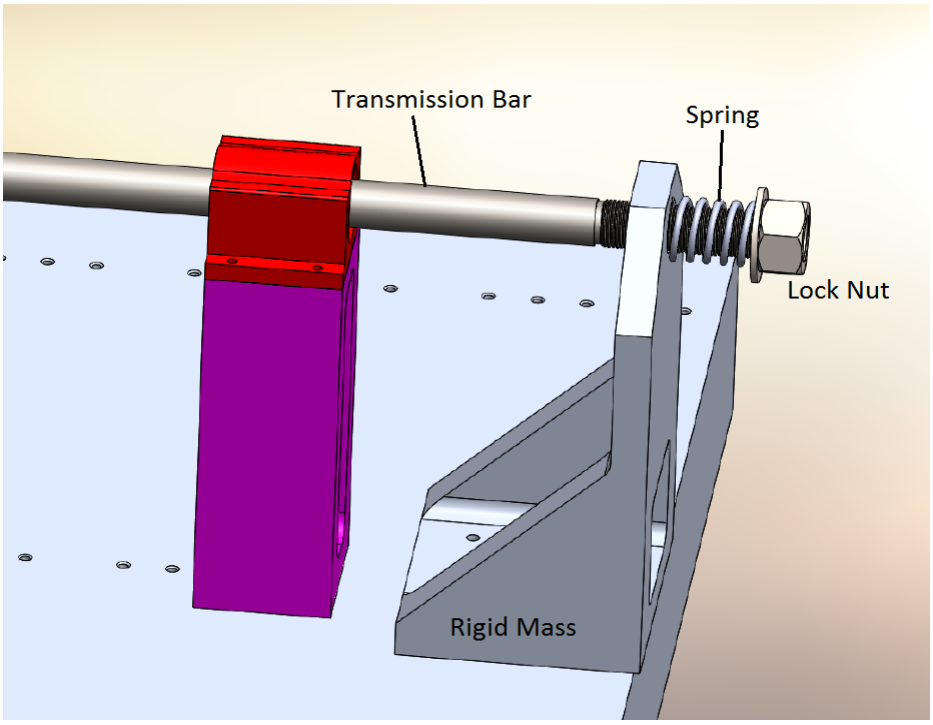

(d)

Figure 5. Modifications to Kolsky tension bar for high-temperature testing. c) cooling system; d) pre-tension load system

5(d), was developed to prevent the specimen from buckling during heating. The spring was placed between a rigid mass and a flange screwed onto the free end of the transmission bar. Screwing the flange toward the rigid mass compresses the spring and in turn generates a tension load in the tension bar system. Another rigid mass was placed against the gun barrel (Fig. 4) to prevent the bar system from moving backwards when the whole bar system is pre-loaded in tension [30]. In this study, the spring was set to generate a pre-tension load of approximately 18N which is sufficient to straighten the iridium specimen during heating but insufficient to produce significant tensile strain on the iridium specimen.

Another high temperature testing issue is thermal softening of the specimen. In general, the flow stress in metallic materials significantly decreases at elevated temperatures, which results in a very weak transmitted signal in Kolsky bar experiments (Eq. (8)). In order to measure the weak transmitted signal with relatively high resolution, a pair of semiconductor strain gages was used to replace the regular resistor strain gages on the transmission bar. The semiconductor strain gages had a gage factor of 139, which is approximately 70 times more sensitive than the regular resistor strain gages.

As mentioned earlier, it has been more challenging to use the reflected wave signal to measure the specimen deformation in Kolsky tension bar experiments due to the complex fixtures that connect the tensile specimen to the bar ends. In this study, we developed a novel splitting-beam laser extensometer to measure the displacements at both specimen ends independently. The specimen strain was thus calculated with the displacement measurements. Combining the measurements of the semiconductor strain gages (Eq. (8)) and the laser system for specimen stress and strain histories, respectively, yields the stress-strain curve of the specimen under investigation.

2.2. Development of Splitting-Beam Laser Extensometer

The general concept of the splitting-beam laser extensometer technique is shown in Fig. 6 [31]. A 5 mW line laser and optical lens system were applied to a Kolsky bar setup to generate a collimated sheet laser scanning on the specimen gage section and portions of the incident and transmission bars. The laser beam was then divided into two independent sections using a right-angle prism mirror. The apex of the right angle serves as a virtual reference line diverting the laser into two opposite directions. Each portion of the laser was focused on a laser detector (Thorlabs PDA 36A) to track the motion of either the incident or transmission bar end. This design prevented the possible interference between the two laser channels. The displacement measurements at the incident bar/specimen and specimen/transmission bar interfaces were measured independently. The Thorlabs laser detector had a tunable resolution with a correlated frequency response. At the bandwidth of 100 kHz or higher that is usually required for Kolsky bar experiments [7], the laser detector was capable of measuring the displacement with a resolution of approximately 100 nm, which corresponds to a strain resolution of 0.0016% for a tensile specimen with a gage length of 6.35 mm. The utilization of two independent laser detection systems allows setting the resolutions and bandwidths for displacement measurement at the incident bar/specimen and specimen/transmission bar interfaces independently. In Kolsky

bar experiments, the transmission bar moves at a lower velocity than the incident bar. Therefore, the laser detector for the measurement at the transmission bar side is recommended to be set with a higher resolution due to the smaller displacement output. This improves the accuracy for small-strain measurement without sacrificing the superiority of traditional laser extensometers on large-strain measurement.

Before dynamic testing, the laser system was carefully calibrated to determine the linearity and sensitivities. Figure 7 shows typical calibration curves for the laser detector 1 (at incident bar end) and detector 2 (at transmission bar end) with different resolutions (gain levels). Both detectors exhibit excellent linearity in the calibration curves but different resolutions due to different gains, which provides more flexibility to improve the displacement measurement resolutions at both ends of the specimen.

After the specimen displacement (ΔL) is measured, the specimen strain can be directly calculated as

$$\varepsilon = \frac{\Delta L}{L_s} \tag{9}$$

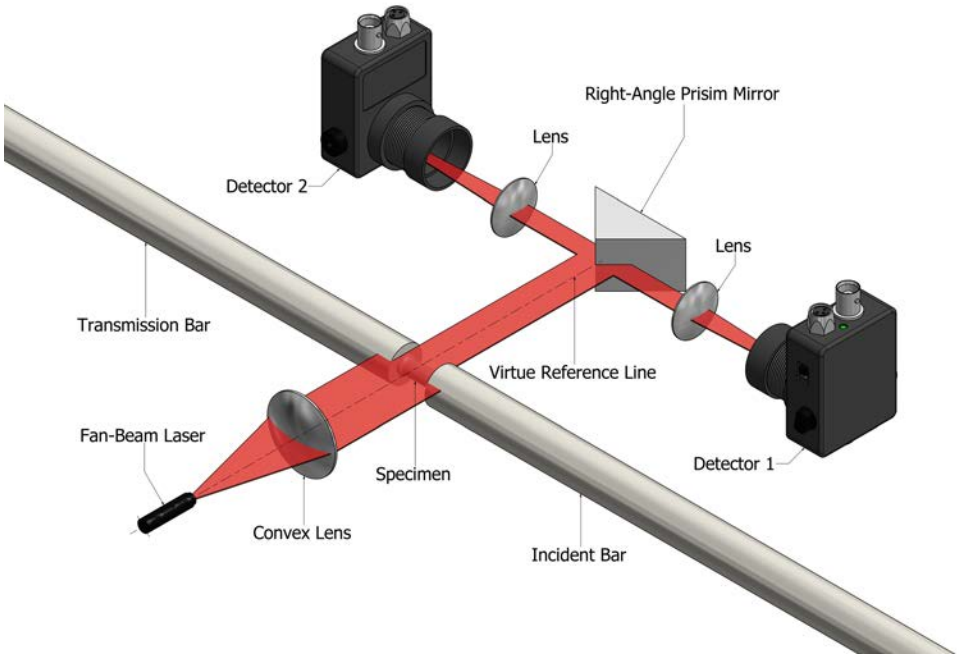

Figure 6. Schematic of laser extensometer.

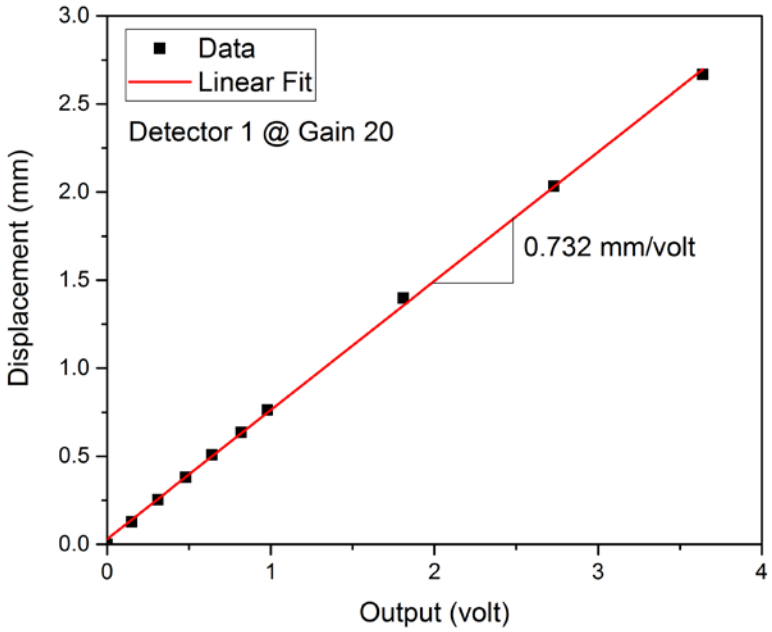

(a)

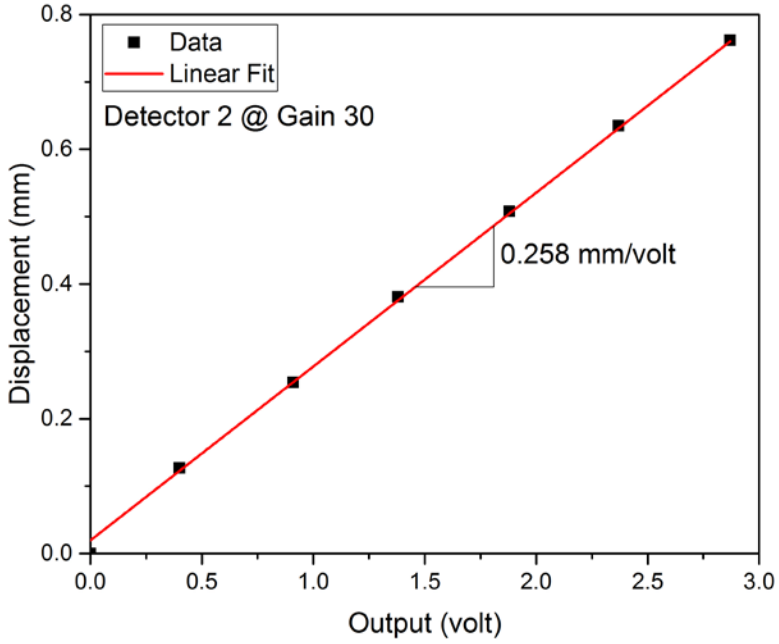

(b)

Figure 7. Typical laser-extensometer calibration curves. a) detector 1; b) detector 2

This page intentionally left blank.

3. DYNAMIC HIGH-TEMPERATURE TENSILE EXPERIMENTS

In this section, the dynamic high-temperature tensile experimental procedure on the DOP-26 iridium alloy at temperatures of 750°C and 1030°C and two different strain rates at each temperature are presented.

3.1. Iridium Alloy Specimen Preparation

The iridium alloy specimens were prepared by ORNL. The iridium tensile specimens were removed from prime DOP-26 alloy blanks using electrical discharge machining (EDM) with a zinc-coated brass wire. The specimens were ground to remove the residual EDM layer, and then deburred and polished. All specimens were acid cleaned and then heat treated at 1375°C ± 25°C for 1 hour ± 10 minutes in vacuum (1×10^{-4} torr). The tensile specimens had a thickness of 0.66 mm, a width of 2.54 mm, and a gage length of 6.35 mm. The detailed dimensions of the iridium specimens used in this study are shown in Fig. 8. Several indentation marks have also been made on the back surface of the tensile specimen to estimate the failure strains after the dynamic tests.

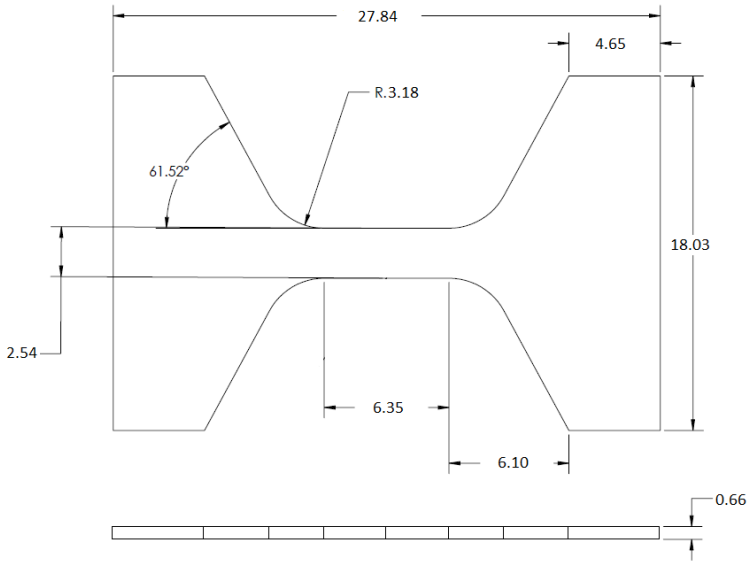

Figure 8. Iridium tensile specimen design.

3.2. High-temperature Control

In order to check the temperature uniformity in the specimen during heating, three thermocouples were attached to the gage section of an iridium specimen: one was placed in the center and the other two were placed very close to each end of the specimen, as shown in Fig. 9(a). Figure 9(b) shows the temperature histories from the three thermocouples when the induction heater was programmed to heat the specimen to 750°C. The thermocouple signals were noisy with high frequencies that were caused by the electromagnetic field in the induction coil. In order to provide clearer temperature readings, a 10Hz digital filter was applied to the thermocouple signals, the results of which are also shown in Fig. 9(b). It is noted that the full heating process has been recorded and is shown in Fig. 9(b). However, it takes much less time, usually 3-4 seconds (called "time window of testing" here), to complete the whole dynamic testing procedure from firing to testing, as marked in Fig. 9(c). The temperatures were very consistent during the heating process as indicated by the thermocouples in three different locations. The results within the time window of testing demonstrate the reasonable uniformity of the temperature across the whole specimen gage section (757 ± 17°C). In addition, we attached a thermocouple to the fixture surface to compare with the temperatures measured with the thermocouples on the specimen. The temperature histories were also consistent. In actual iridium alloy testing, only one thermocouple was attached to the fixture surface under the specimen, as shown in Fig. 5(a), to avoid microstructural changes in the specimen due to spot welding of the thermocouple to the surface.

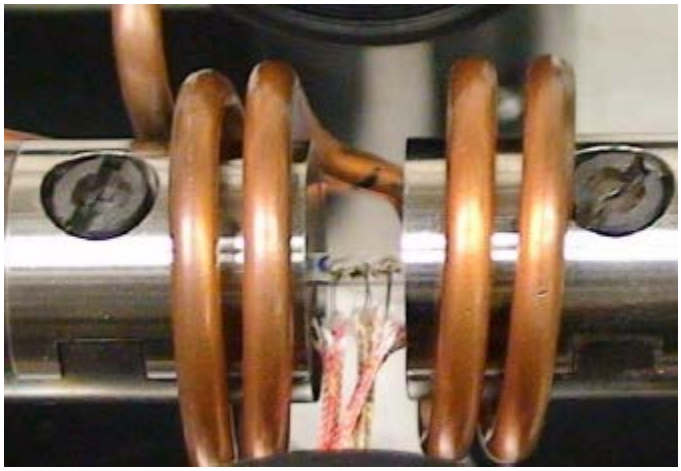

(a)

Figure 9. Temperature histories on the iridium specimen at different locations. a) photograph of thermocouples at different locations on the specimen surface

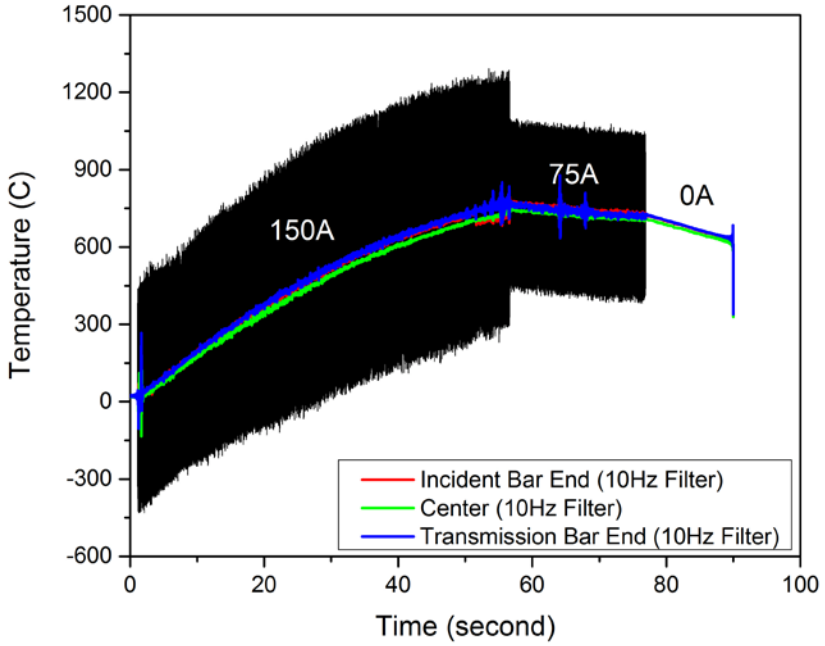

(b)

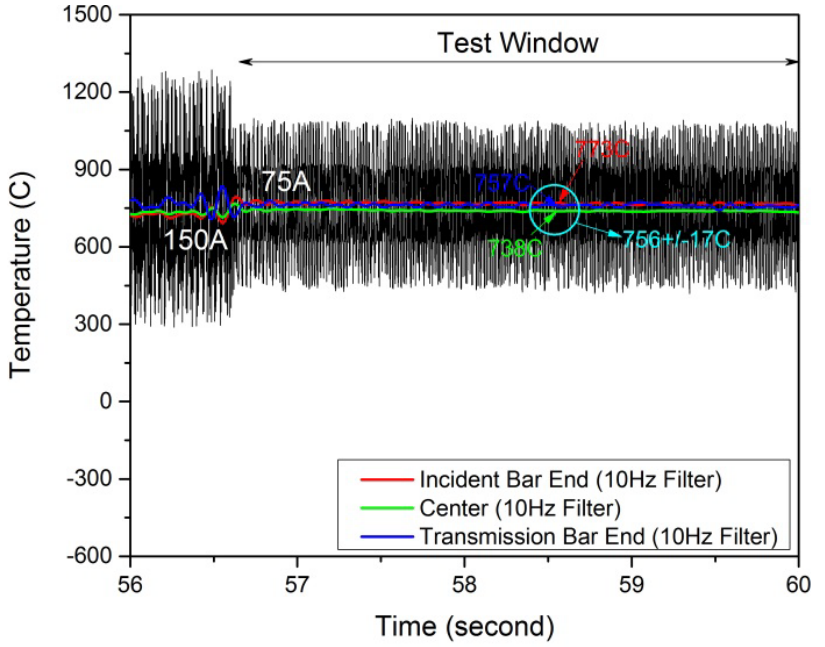

(c)

Figure 9. Temperature histories on the iridium specimen at different locations. b) temperature histories during heating process; c) temperature histories within a test window

3.3. Dynamic High-temperature DIC Approach

A reliable Kolsky bar experiment requires uniform deformation in the specimen over the entire duration of loading. In most cases, the uniform deformation can be represented by stress equilibrium in the specimen that is usually evaluated with the comparison of forces/stresses at both ends of the specimen. The stresses at the incident bar/specimen and specimen/transmission bar interfaces can be calculated with Eqs. (3) and (4), respectively. However, in Kolsky tension bar experiments, the complicated specimen fixtures/adapters such as the ones used in this study make the reflected pulse unreliable to calculate the stress at the incident bar/specimen interface. In this case, the stress equilibrium or strain uniformity in the tensile specimen cannot be directly assessed. In this study, we used a dynamic high-temperature DIC approach to evaluate the validity (uniformity of deformation) of high-temperature Kolsky tension bar experiments on the iridium alloy.

Figure 10 shows the Phantom V12.1 high-speed digital camera and LED lighting system used in this study.

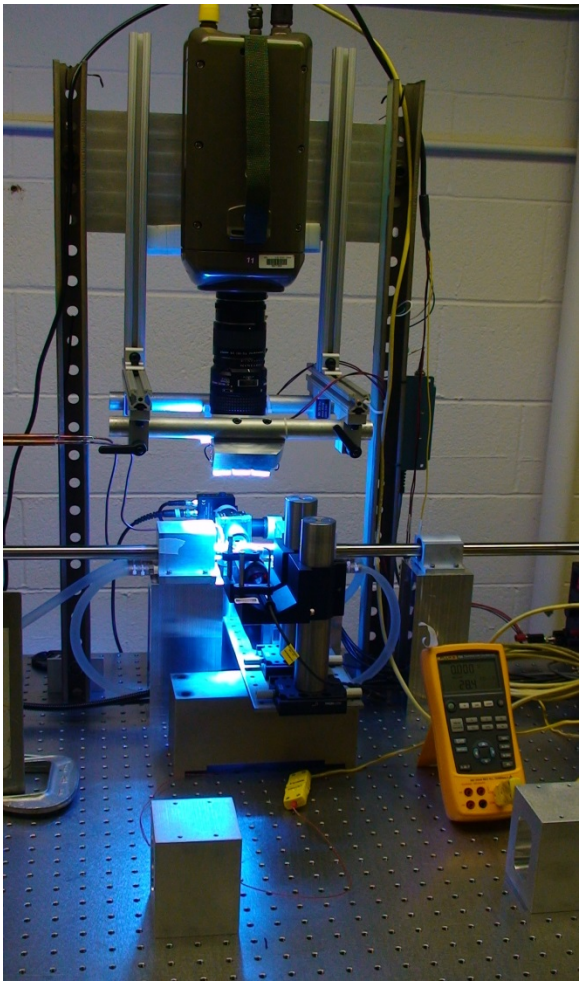

Figure 10. High-speed digital camera and lighting for DIC analysis.

It is a challenge to apply conventional DIC techniques to dynamic high-temperature tests. For example, the regular paint commonly used to generate patterns in conventional DIC techniques may not be applicable to high temperatures particularly when the temperature is as high as 1030°C. Furthermore, the regular painted pattern may spall due to significantly high acceleration/deceleration under high-rate impact loading. In this study, we used a sand blast to generate random roughness on the surface of the iridium specimen. The surface roughness reflects various amounts of light back to the high-speed camera, generating high-speed images with reasonable contrast for image correlation. In this approach, the sand blast pressure was set at 20 psi using ~10-μm-diameter silica particles against the surface of the iridium specimen. This generated random depressions ~1 μm in size on the surface of the specimen.

Figure 11 shows selected high-speed images of the specimen surface during dynamic loading at 870 s^{-1}/920°C. The images were taken with the Phantom v12.1 high-speed digital camera at a speed of 60,021 frames per second. The bright portion in the images represents the gage section of the specimen under dynamic tensile load. With increasing time, the bright portion became longer while the specimen was being stretched. The images in Fig. 11 showed decreasing but still reasonable contrast for DIC analysis. The corresponding full field deformation history of the specimen, which was calculated with the DIC analysis, is shown in Fig. 12. It is observed that a nearly uniform deformation has been achieved in the specimen within the first 16.7 μs. The specimen continued to undergo uniform deformation until $t = 349.9\mu s$ when localized necking began. The specimen strain at the onset of localized necking was 43% (Fig. 12). It should be noted that the specimen did not fail by the end of the first dynamic loading, thus the actual failure strain should be larger than 43%.

Figure 13 shows the displacement history along the gage section. Under dynamic tensile loading, the whole specimen was observed to move along the loading direction. However, the specimen end that was attached to the incident bar moved much faster than the other end attached to the transmission bar such that the specimen was significantly elongated. The nearly linear curves of displacement versus time shown in Fig. 13 indicate that the specimen was subjected to nearly uniform deformation in the gage section during dynamic loading. The average strain by the end of the first loading can be estimated with the slope of the last displacement curve, $\varepsilon = 60/165 = 0.363$, which falls into the strain range between 33% and 43% as shown in the last image in Fig. 12.

Again, the iridium tensile specimen did not fail during the first loading but eventually failed after multiple dynamic loadings during a single Kolsky tension bar test. Figure 14 shows the images of the iridium tensile specimen after dynamic testing. As mentioned in section 3.1, several indentation marks were made on the back surface of the tensile specimen. Post-test examination of the distances between these indentation marks provides an estimate of the strains (including total) to failure which are listed in Table 1. Table 1 shows the specimen failed between indentation marks 2 and 3. The specimen strain was localized (necked) in this region. The neighboring region (1-2) to the necked region had a significantly higher strain of 0.586, which indicates the actual engineering failure strain should be higher than 0.586. The uniformly deformed regions (4-5, 5-6, and 6-7) had strains varying from 0.377 to 0.392 with an average strain of 0.386 at failure. The total strain over the entire gage length was 0.438, which is also

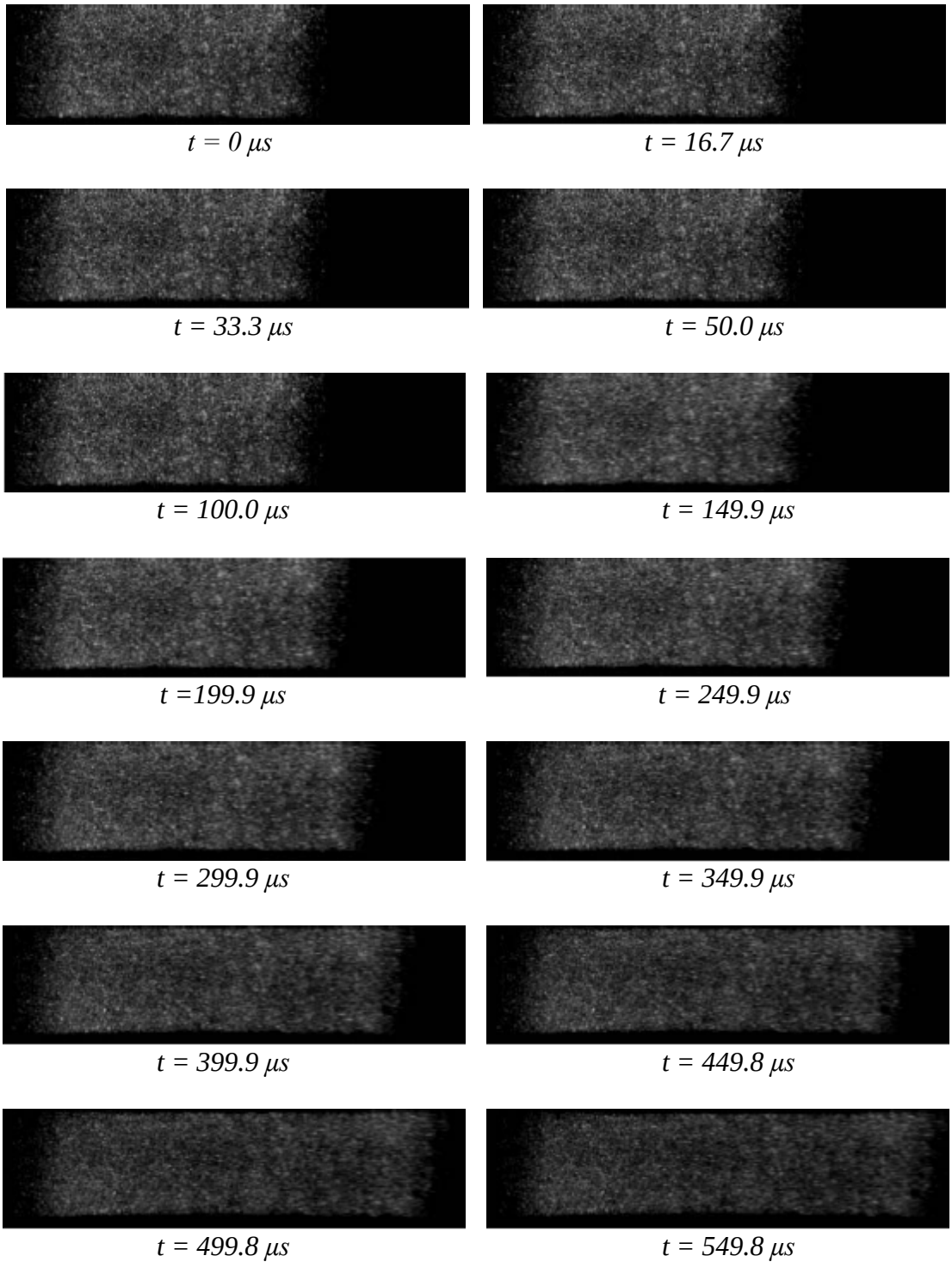

Figure 11. High-speed images of specimen deformation.

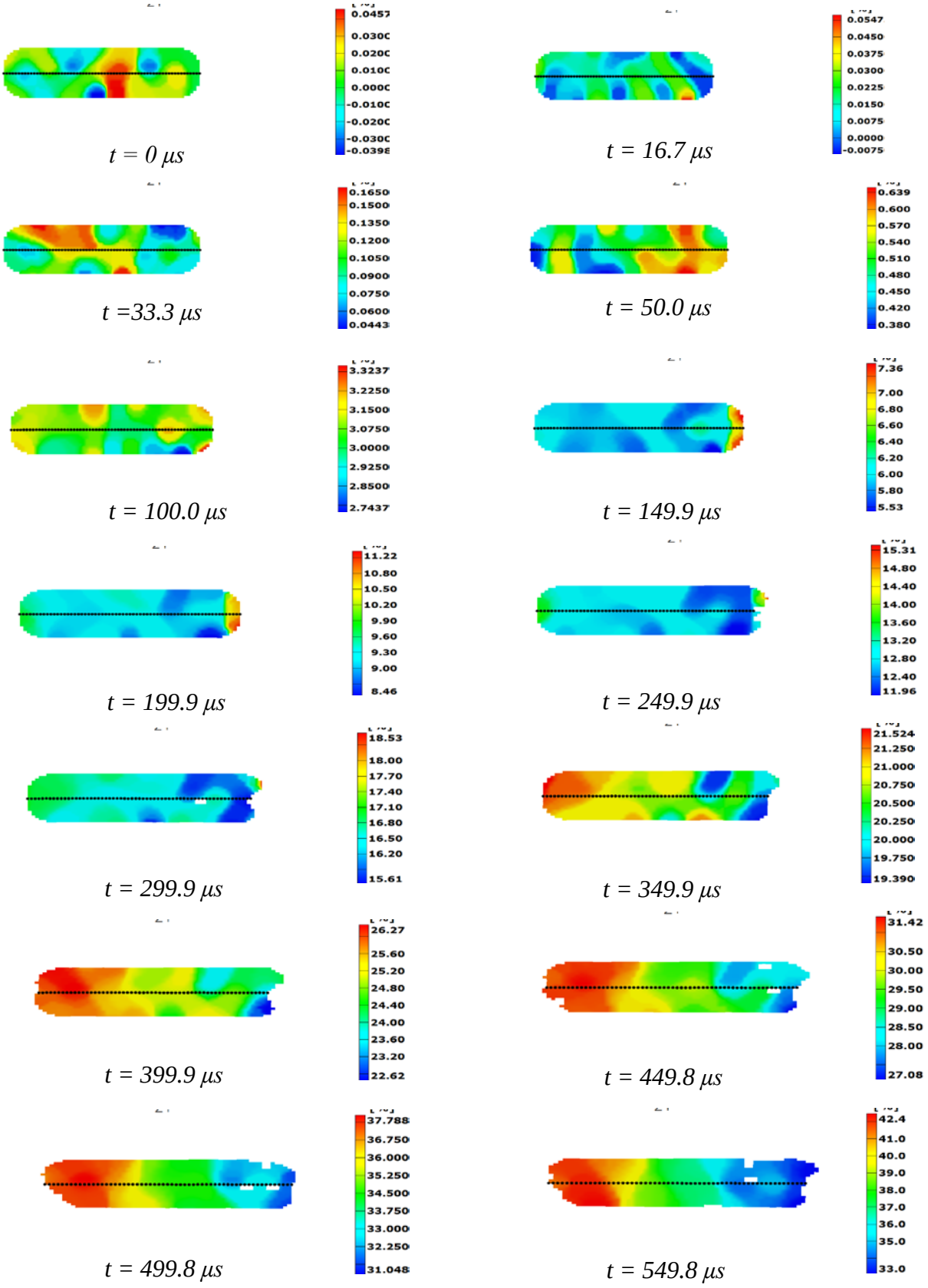

Figure 12. DIC results (engineering strain) on the specimen deformation.

reasonable when compared with the DIC results.

In summary, the DIC results were shown to be valid in terms of uniform deformation before necking occurred in the specimen. However, the DIC data may not be sufficiently accurate for calculating precise stress-strain response. In this study, the DIC was therefore used to validate the testing conditions only. In addition, the lighting for DIC may interfere with the laser system that was used to precisely measure the specimen deformation. Therefore, the DIC was not applied for actual material testing in this study.

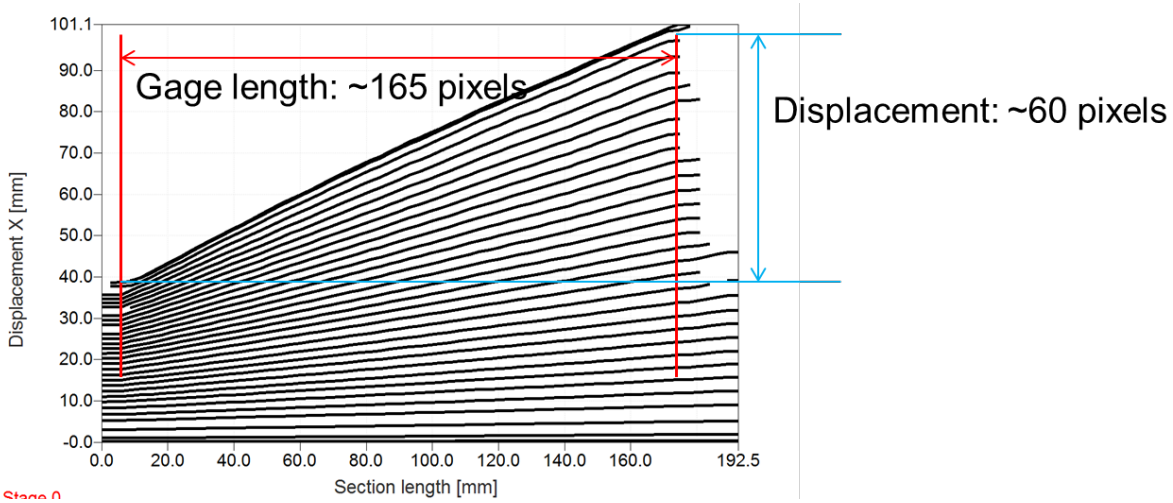

Figure 13. DIC results on the specimen displacement histories.

Figure 14. Photograph of the iridium specimen after dynamic test.

Table 1. Estimate of specimen strain after dynamic failure

Indentation Marks	Before Test (mm)	After Test (mm)	Strain
1-2	0.8903	1.4121	0.586
2-3	0.8890	N/A	N/A
3-4	0.8890	1.2871	0.448
4-5	0.9233	1.2832	0.390
5-6	0.8865	1.2338	0.392
6-7	0.8814	1.2140	0.377
Total	4.4705*	6.4302*	0.438*

**The distance and deformation of 2-3 were excluded.*

3.4. Dynamic High-Temperature Tensile Experiments

Figure 15 shows typical strain gage signals on the incident and transmission bars for the incident, reflected, and transmitted waves at a test temperature of 1030°C. As shown in Fig. 15, the transmission bar strain was low (only 15 microstrains) due to the low strength of the iridium specimen at such a high temperature. However, high resolution measurement of the low transmitted signal was achieved by using high sensitivity semiconductor strain gages. Again, since the reflected pulse was not reliable for specimen strain measurement, we used the laser system (Fig. 6) to directly track the movements of the specimen ends that were attached to the incident and transmission bars. The laser outputs are shown in Fig. 16. Figure 16 clearly shows significant change in the laser output for the front end (on the incident bar side) but no significant change for the back end (on the transmission bar side). This is because the transmitted force was too small to generate significant displacement on the transmission bar side even though a higher gain/resolution was set.

Figure 17 shows the thermocouple output during dynamic loading. The thermocouple signal was noisy due to the electromagnetic field generated by the induction coil. We applied a 100 kHz digital filter and the result was plotted in red in the same figure. The results showed in Fig. 17 demonstrate that the temperature was maintained as a constant (1033°C) during dynamic loading. It is noted that the induction heater used in this study was in open-loop operation, which made it difficult to exactly control the specimen temperature as desired. In this study, the actual testing temperatures were controlled at nearly constants but within 5% of the desired temperatures.

The engineering stress and strain histories in the specimen, which were calculated with Eqs. (8) and (9), respectively, are shown in Fig. 18. The strain rate was then calculated with the slope of

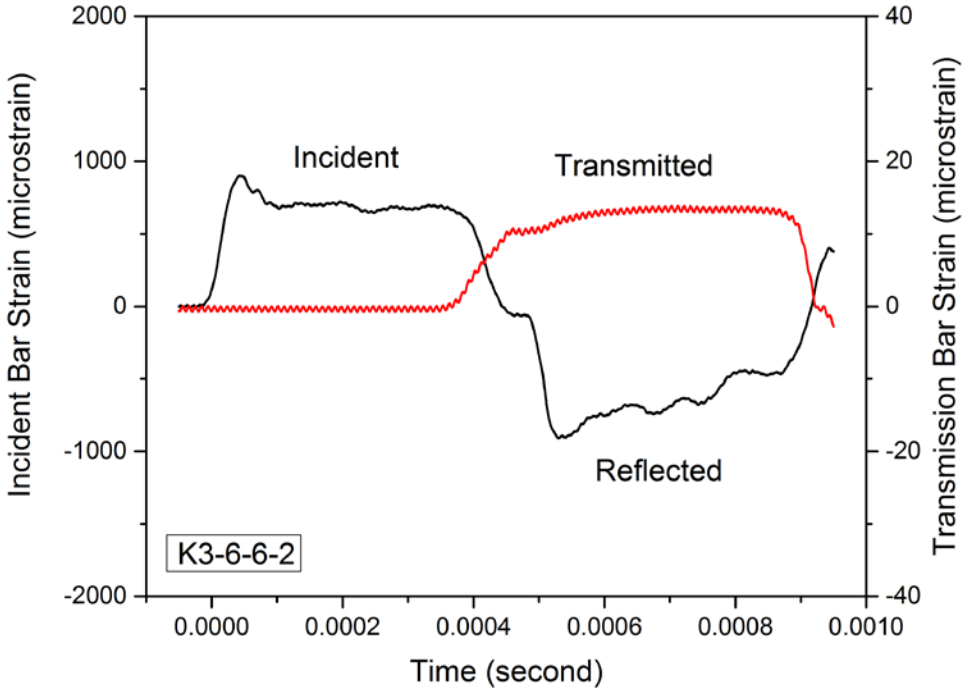

Figure 15. Typical strain-gage signals during dynamic loading.

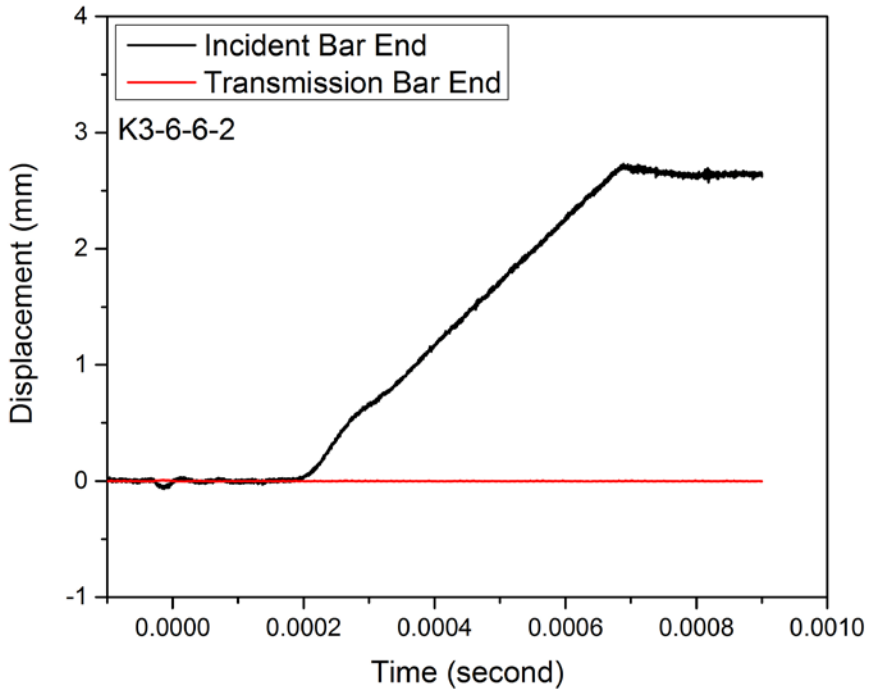

Figure 16. Laser extensometer signals.

the strain history as a nearly constant of 860 s^{-1}. It is noted that when the reflected pulse became unreliable, it was difficult to compare the force histories at both ends of the specimen for force/stress equilibrium checks. However, the preliminary test with DIC approaches presented in section 3.3 demonstrated the specimen deformed uniformly which represented stress equilibrium during dynamic loading.

Based on the stress and strain histories shown in Fig. 18, the tensile stress-strain response of the iridium alloy specimen was obtained at 860 s^{-1}/1030°C (see Fig. 19). Significant oscillations were observed in the raw stress-strain curve because of the effect of the electromagnetic field generated by the induction coil on the highly-sensitive semiconductor strain gage signals. The raw stress-strain data was then filtered to remove the oscillations, the result of which is also shown in Fig. 19. It is noted that the sudden drop in the stress-strain curve is the result of unloading and does not represent the failure of the specimen.

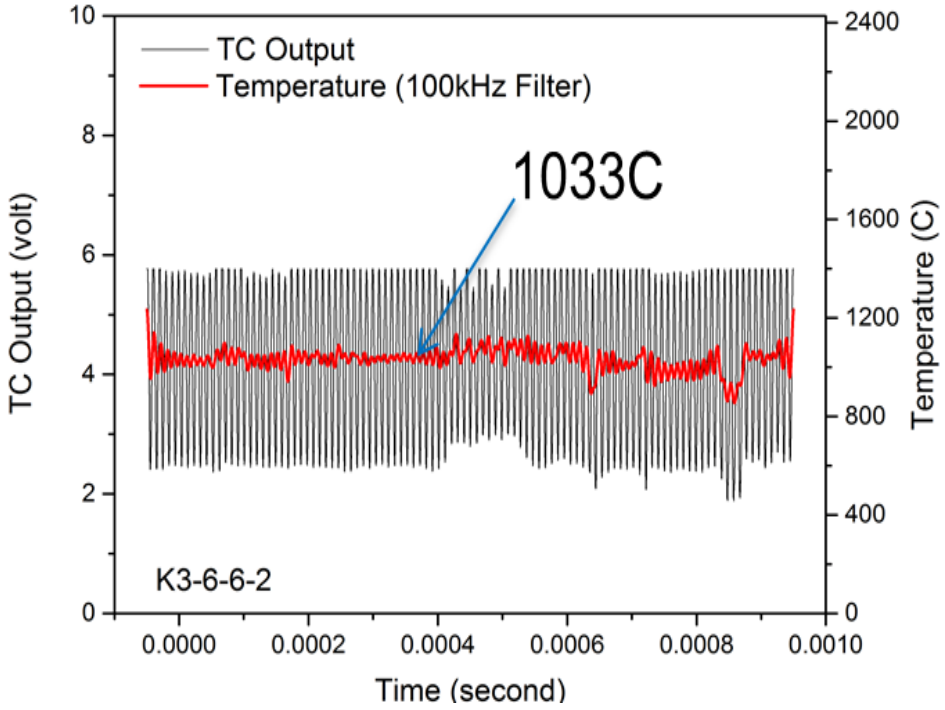

Figure 17. Temperature history.

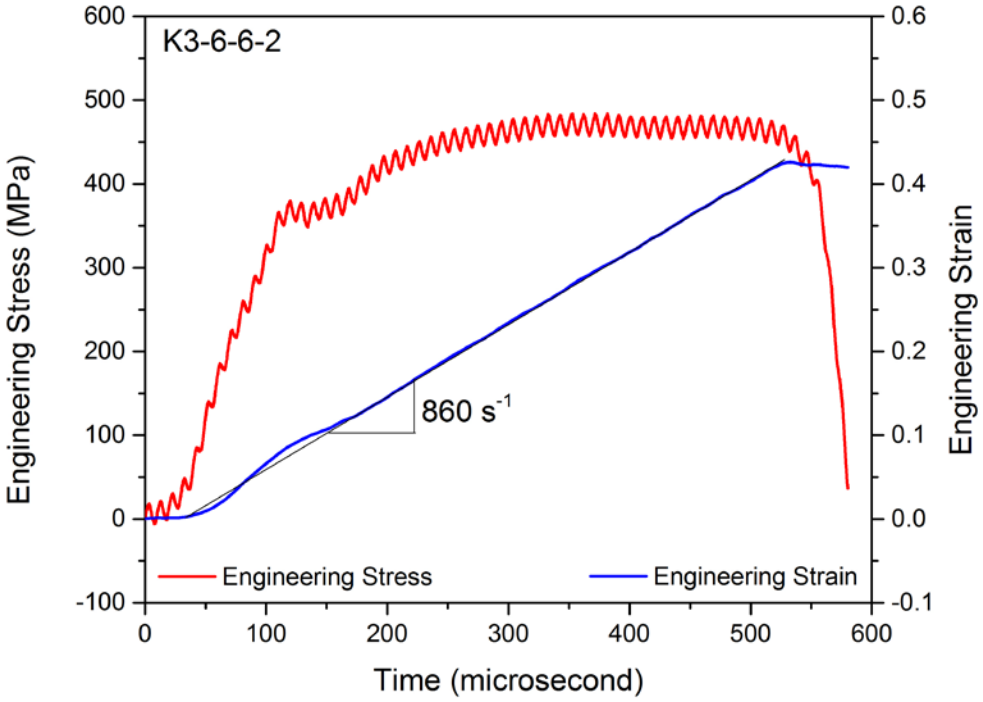

Figure 18. Stress and strain histories.

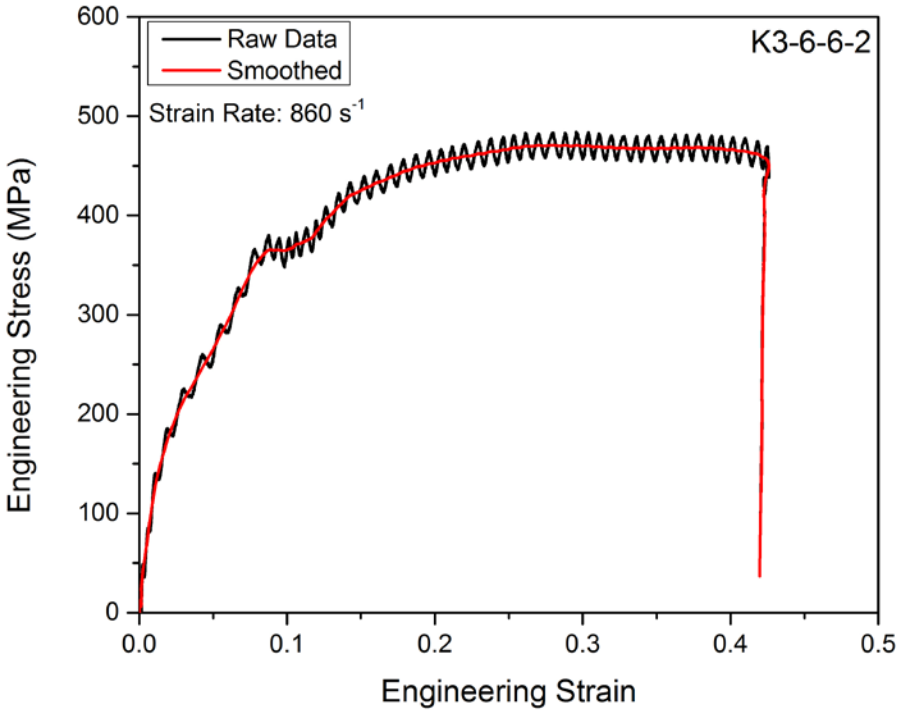

Figure 19. Engineering stress-strain curve at 860 s^{-1}/1030°C.

4. EXPERIMENTAL RESULTS AND DISCUSSION

Following the same procedure, the DOP-26 iridium alloy was characterized in tension at two different strain rates (1000 and 3000 s^{-1}) and temperatures (750 and 1030°C). Three experiments were run at each condition. In this section, the dynamic high-temperature tensile characterization results of the iridium alloy are presented and discussed.

4.1. Experimental Results

Figure 20 summarizes the tensile stress-strain curves of the iridium alloy at different strain rates and temperatures. At similar testing (temperature and strain rate) conditions, the iridium specimens exhibit reasonable repeatability in the tensile stress-strain response, except for the specimen GR9-14-3-2 at 735°C/3400 s^{-1}. The specimen GR9-14-3-2 exhibits a significant smaller failure strain than the other two (GR9-14-4-1 and GR9-14-4-2). No explanation for this has been found. Based on review of the specimen fabrication records and post-test specimen examination, the low failure strain for specimen GR9-14-3-2 does not appear to be attributable to sample preparation imperfections or microstructural anomalies. The tensile stress-strain curves at similar testing conditions were averaged, except for the specimen GR9-14-3-2, and the mean curves were used as the representative tensile stress-strain response at specific temperature/strain rate conditions. The mean engineering stress-strain curves of the iridium alloy in tension are shown in Fig. 21.

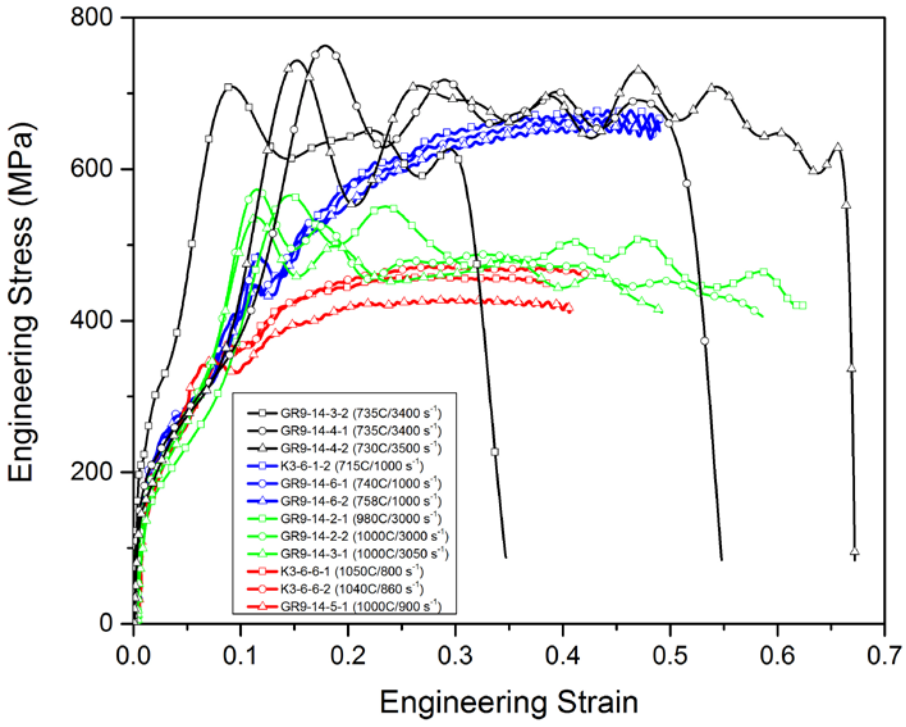

Figure 20. Engineering stress-strain curves of the iridium alloy at various temperatures and strain rates.

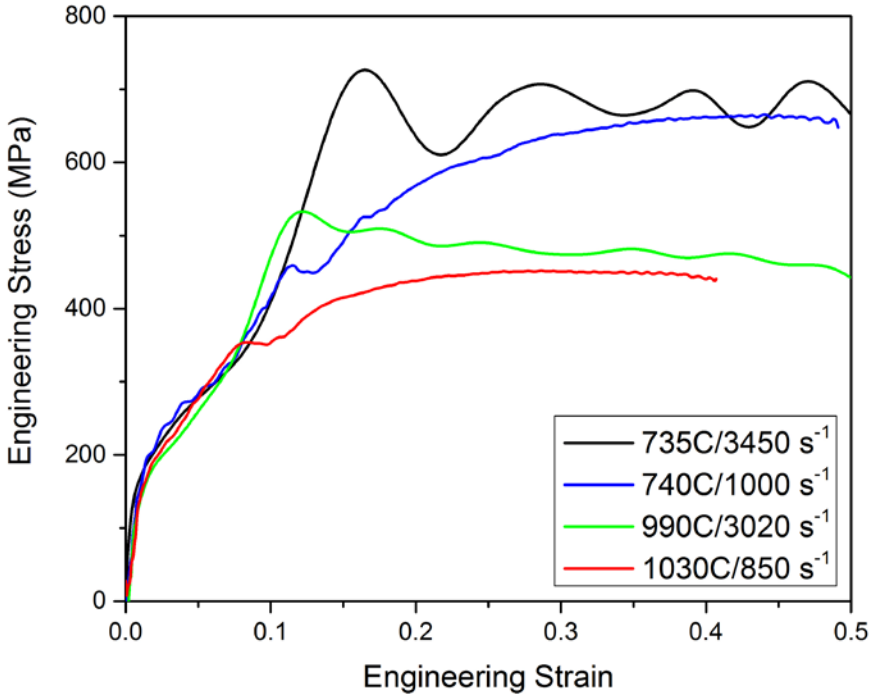

Figure 21. Engineering mean stress-strain curves of the iridium alloy in tension at various temperatures and strain rates.

It is noted that, due to the superior ductility of the iridium alloy at elevated temperatures, the specimens did not fail during the first dynamic tensile load except for the testing condition of 735°C/3450 s^{-1}. At the condition of 735°C/3450 s^{-1}, the specimens possessed engineering failure strains varying between 0.5 and 0.7. However, the engineering failure strains might not represent the actual failure strains since significant strain localization due to necking occurred in the specimens before failure. Therefore, the stress-strain curves are plotted up to 0.5 engineering strain in Fig. 21. The dynamic high-temperature stress-strain curves of the iridium alloy show different profiles from quasi-static curves [4]. All stress-strain curves show an initial elasticity followed by significant work hardening behavior when the strain is below 10%. This phenomenon may be related to a change in deformation mechanism at high strain rates and elevated temperatures, which is still under investigation. Furthermore, when the strain is below 10%, the stress-strain curves show neither strain-rate nor temperature effects. When the strain increases, the stress-strain curves show plastic flow with significant strain-rate and temperature effects. The flow stresses at the strains greater than 10% and similar strain rates decrease when the temperature increases from 750 to 1030°C, showing significant thermal-softening behavior. At the same temperature, the flow stresses increase when the strain rate increases from 1000 to 3500 s^{-1}, showing positive strain-rate sensitivity. In addition, it seems the tensile stress-strain curve possesses more oscillations when the strain rate becomes higher.

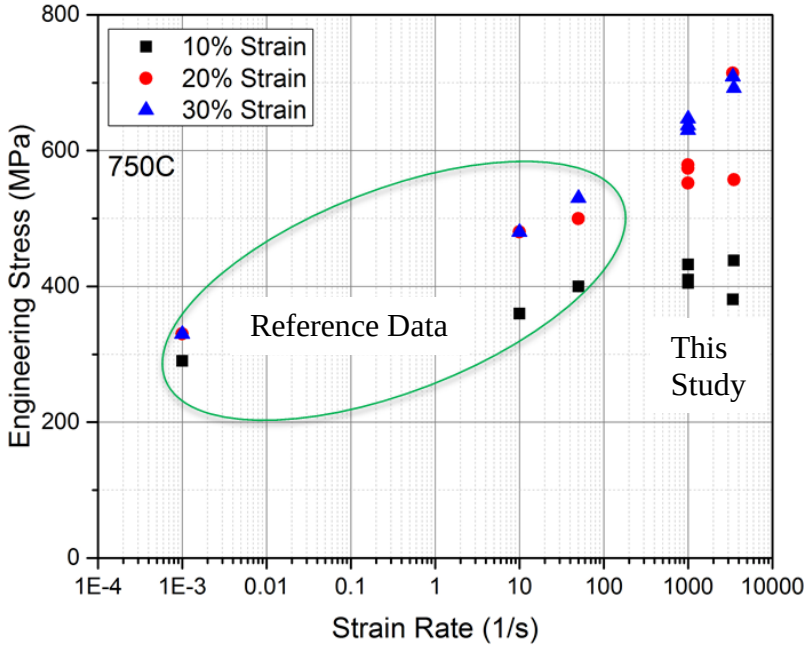

(a) 750°C

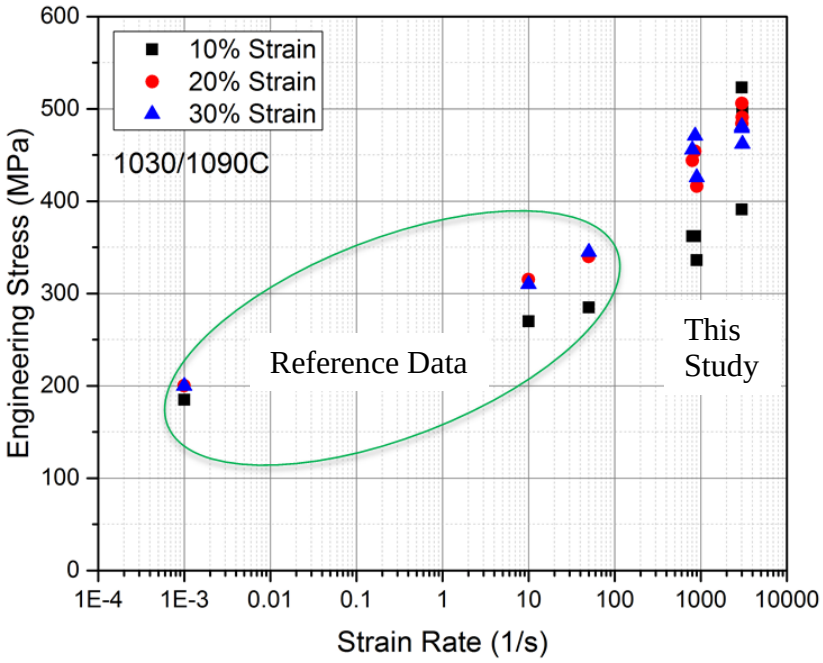

(b) 1030/1090°C

Figure 22. Strain-rate effect. a) 750°C; b) 1030/1090°C

Table 2. Dynamic testing conditions and failure strain estimation

Specimen ID	Temperature (°C)	Strain Rate (1/s)	Strain	
			After First Loading*	Failure Strain**
K3-6-6-1	1050	800	0.385	0.381
K3-6-6-2	1040	860	0.423	0.485
GR9-14-5-1	1030	900	0.402	0.376
K3-6-1-2	715	1000	0.482	0.419
GR9-14-6-1	740	1000	0.488	0.378
GR9-14-6-2	758	1000	0.481	0.393
GR9-14-3-1	1000	3050	0.462	0.418
GR9-14-2-2	1000	3000	0.579	N/A
GR9-14-2-1	980	3000	0.631	0.442
GR9-14-3-2	735	3400	0.292 (failure)	0.231
GR9-14-4-2	730	3500	0.648 (failure)	0.469
GR9-14-4-1	735	3400	0.460 (failure)	0.330

* Determined with the tensile stress-strain curves
** Determined with the indentation marks

Detailed strain-rate effect on the tensile stress-strain response including the quasi-static data presented in [4] is shown in Fig. 22 at two different temperatures (750°C (Fig. 22(a)) and 1030/1090°C (Fig. 22(b)), respectively. The data obtained from the reference [4] are circled and the rest are from this study in both figures. Figure 22 clearly shows significant strain-rate effect on the tensile flow stress of the DOP-26 iridium alloy at both elevated temperatures. The strain-rate sensitivities are slightly different at the two temperatures and are also dependent on the level of strain.

Since most of the iridium specimens did not fail during the first dynamic loading, the indentation marks on the specimen surface were used in this study to estimate the overall nominal failure strains at different testing conditions. The results are listed in Table 2. Table 2 also listed the specimen strains that were calculated from the tensile stress-strain curves after the first dynamic loading, even though the data do not represent the actual failure strains. The strains for the specimens (GR9-14-3-2, GR9-14-4-2, and GR9-14-4-1) that are shown in Table 2 represent the failure strains because these three specimens failed during the first dynamic loading. It is observed that the strains calculated from the stress-strain curves are larger than those estimated with the indentation marks. This is because the indentation marks within the failure region were difficult to detect after dynamic testing. The strains in the failure region, which should be the largest over the entire gage length, were not taken into account in the calculations of the overall specimen failure strain. Therefore, the overall specimen failure strains calculated with the indentation marks were under estimated. Figure 23 shows the photographs of all iridium alloy specimens after dynamic testing. Since the specimens were stretched to large strains, the surface textures of the specimens, particularly in the failure areas, were significantly changed. This complicated identification of the indentation marks after dynamic loading and created uncertainties in some strain calculations.

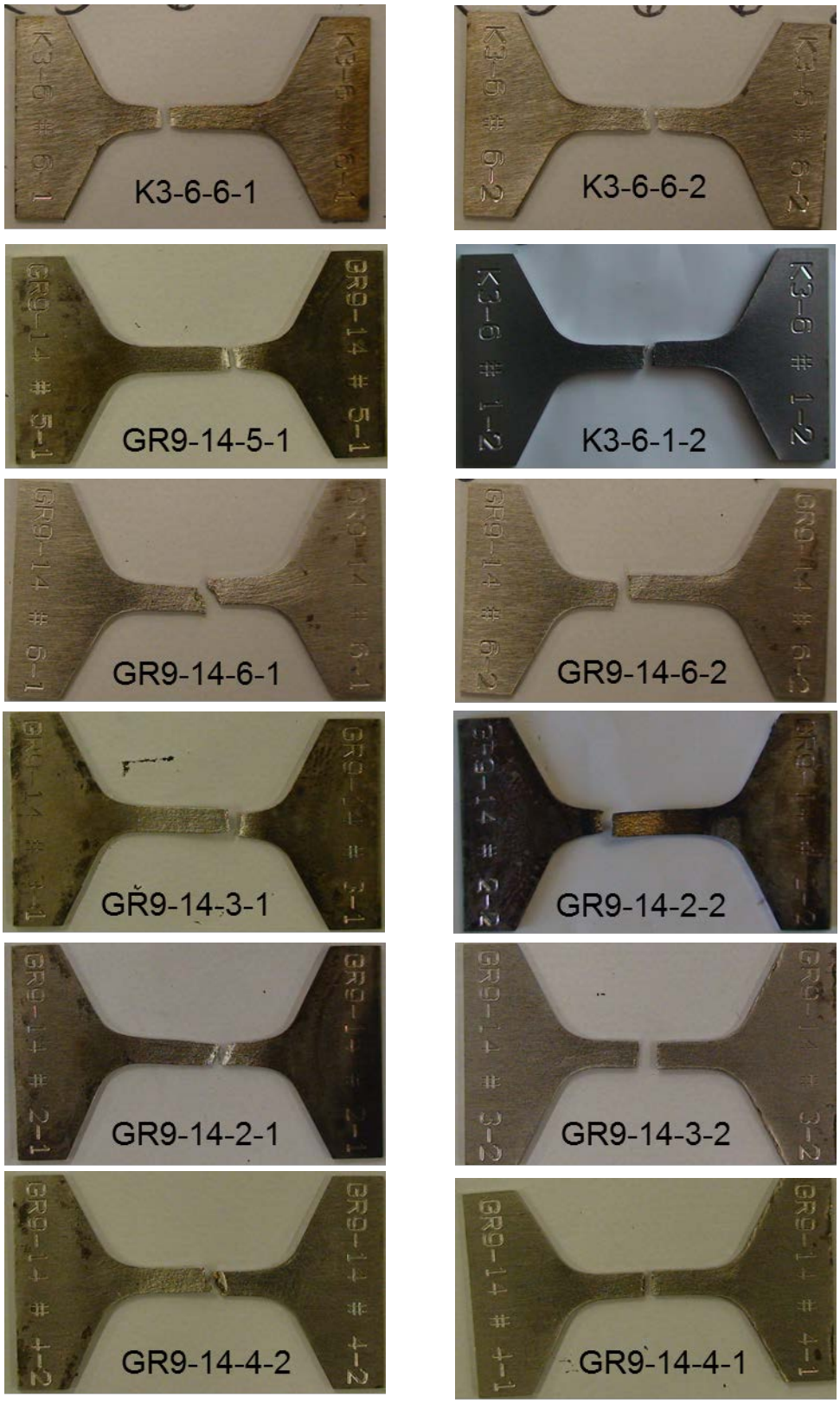

Figure 23. Photographs of the iridium specimens after dynamic tests.

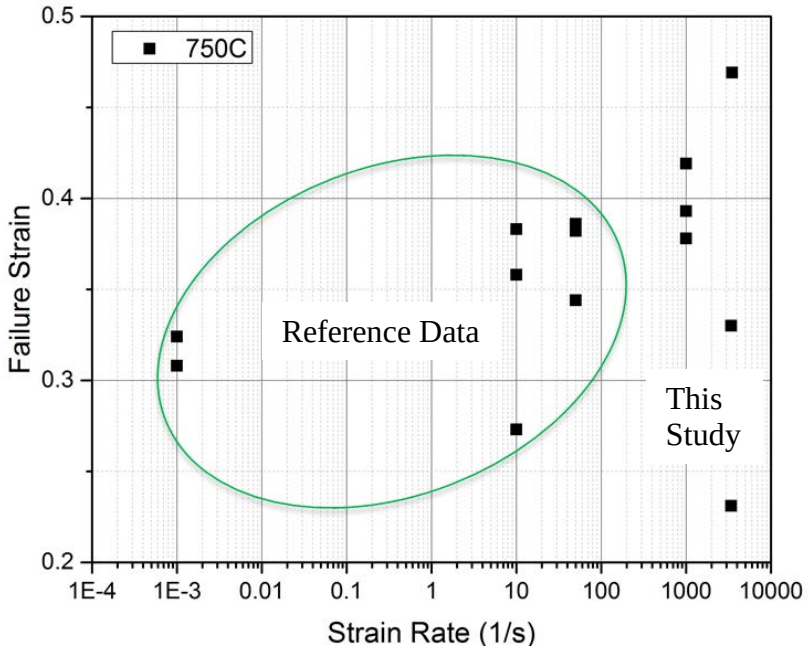

(a) 750°C

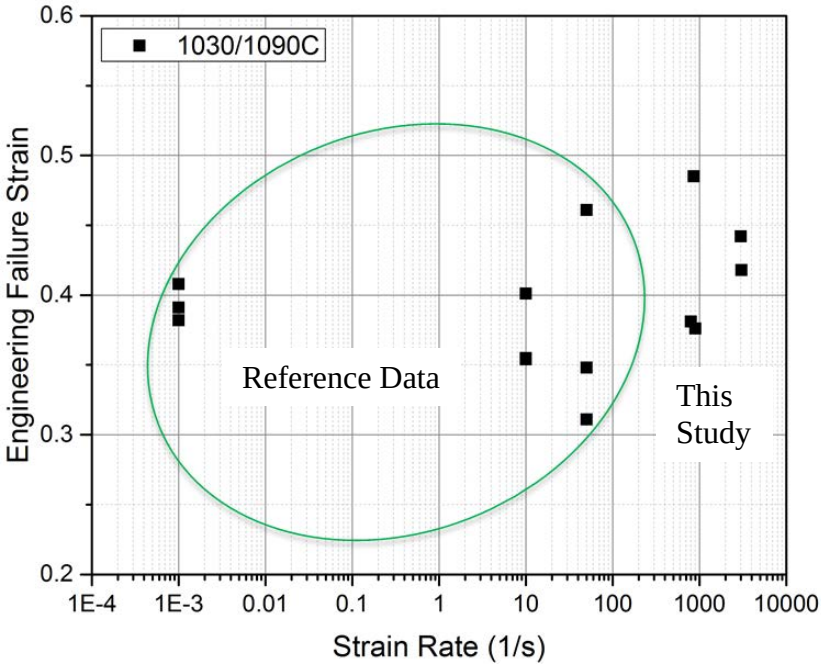

(b) 1030/1090°C

Figure 24. Failure strains obtained in this study and Ref. [4]. a) 750°C; b) 1030/1090°C

In Fig. 24, we also plotted the failure strain data shown in Table 2 and compared them with the circled data that were obtained at lower strain rates [4]. Even though the specimen dimensions used in Ref. [4] are different from this study, the failure strains in Ref. [4] were determined with the same method using the indentation marks. Figure 24 shows that the failure strains obtained from this study are consistent with the data obtained at lower strain rates up to 50 s^{-1} in Ref. [4]. It is noted that the difference in specimen dimensions used in this study and Ref. [4] may generate uncertainties in the overall failure strains. Therefore, the comparison of failure strains shown in Fig. 23 shall be used for reference only.

4.2. Discussion

In this study, the DOP-26 iridium alloy was characterized in tension at high strain rates and elevated temperatures. The same material was also characterized in compression at similar strain rate and temperature conditions [8, 9]. It is reasonable to compare both compression and tensile data to understand the uncertainties of the resultant data which are important for determining the margins in safety analyses. In order to compare the tensile and compression data, the true stress-strain response should be used. Assuming incompressible solids, the true stress (σ_T) and strain (ε_T) can be calculated with engineering measurements, σ_E and ε_E, respectively,

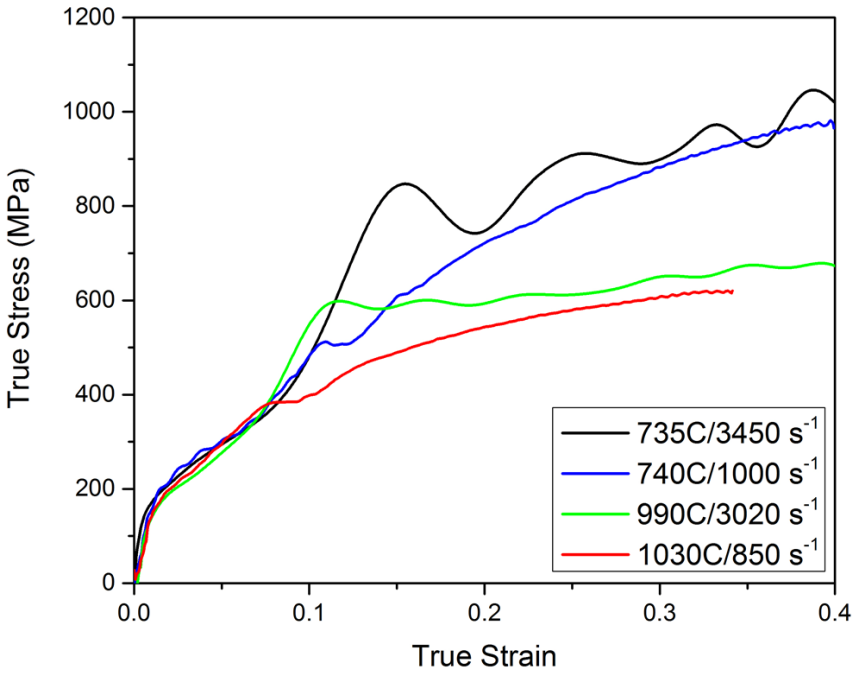

Figure 25. True tensile stress-strain curves.

$$\sigma_T = \sigma_E(1+\varepsilon_E) \tag{10}$$

$$\varepsilon_T = \ln(1+\varepsilon_E) \tag{11}$$

According to Eqs. (10) and (11), the true tensile stress-strain curves at different strain rates and temperatures were calculated and shown in Fig. 25. For the same reason, the true stress-strain curves were calculated only before necking occurred.

The dynamic high-temperature true stress-strain responses of the DOP-26 iridium alloy in tension and compression were compared in Fig. 26. At very similar testing conditions (temperature and strain rate), the compressive stress-strain curves are observed to be above the tensile stress-strain curves by 40-50%. In other words, at the same strains, the true compressive stresses are higher than the true tensile stresses. One possible reason for this deviation is the difference in the stress state of the specimen subjected to dynamic compressive and tensile loading. In the dynamic high-temperature compression experiments, the specimen dimensions were 3 mm in diameter and 0.65 mm in thickness, thus the specimens were not in a uniaxial stress state. The friction between the specimen and the bar ends, even though a super enhanced graphite (SEG) was applied as lubricant, further magnified the deviation. Therefore, the thin disc iridium compression specimen was in triaxial stress and strain states. However, the design of the iridium tensile specimens used in this study brought it closer to a uniaxial stress state than the compression specimens. Therefore, higher flow stresses were generated in the compression specimens with a triaxial stress state than in the tensile specimens with a nearly uniaxial stress state.

In most cases in this study, the iridium specimens did not fail during the first dynamic loading but eventually failed due to multiple cycles of dynamic loading within a single dynamic tensile experiment. Even though the indentation marks provided some information regarding the failure strains, the detailed failure information in terms of strain rate and strain has not yet been experimentally obtained. Due to the high ductility of the DOP-26 iridium alloy at high temperatures, the conventional Kolsky bar techniques may not be capable of obtaining sufficient dynamic failure information. Proper modifications or new techniques are therefore needed to dynamically characterize the iridium alloy to failure at elevated temperatures, which are still in progress.

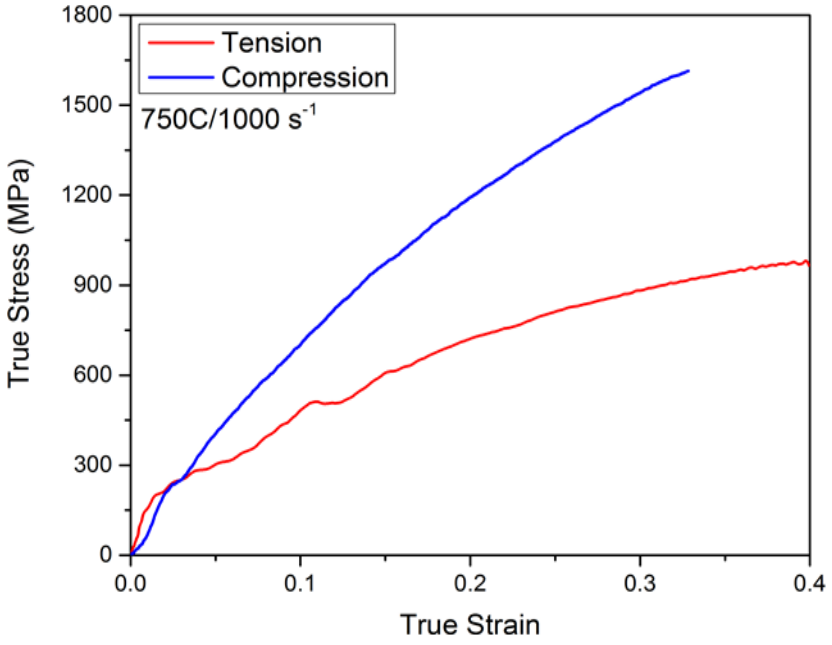

(a)

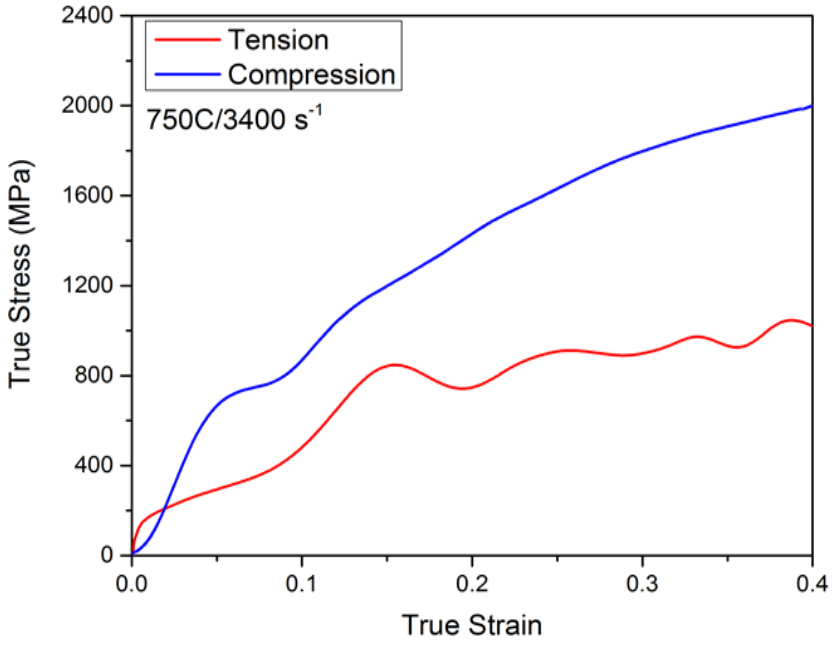

(b)

Figure 26. True tensile stress-strain curves. a) ~750°C/1000 s^{-1}; b) ~750°C/3400 s^{-1}

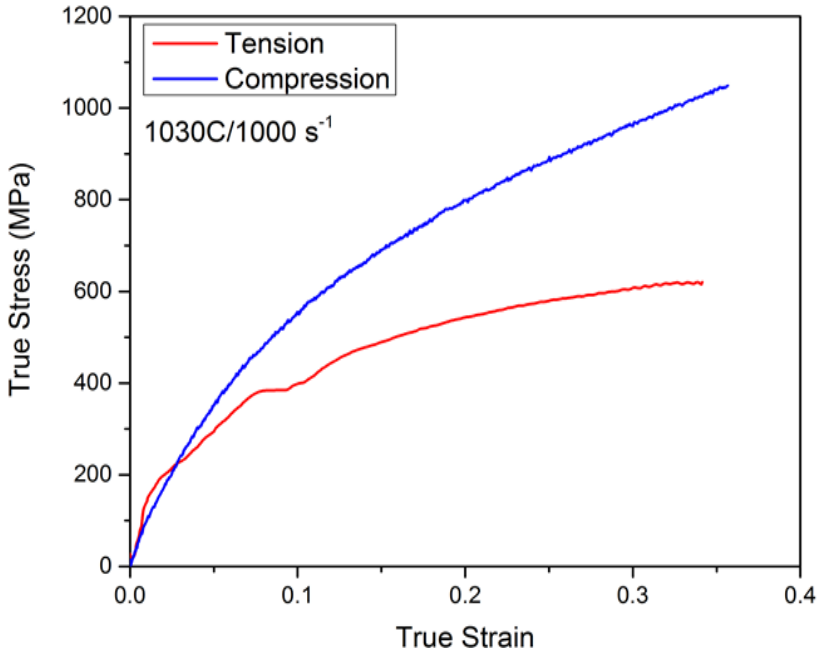

(c)

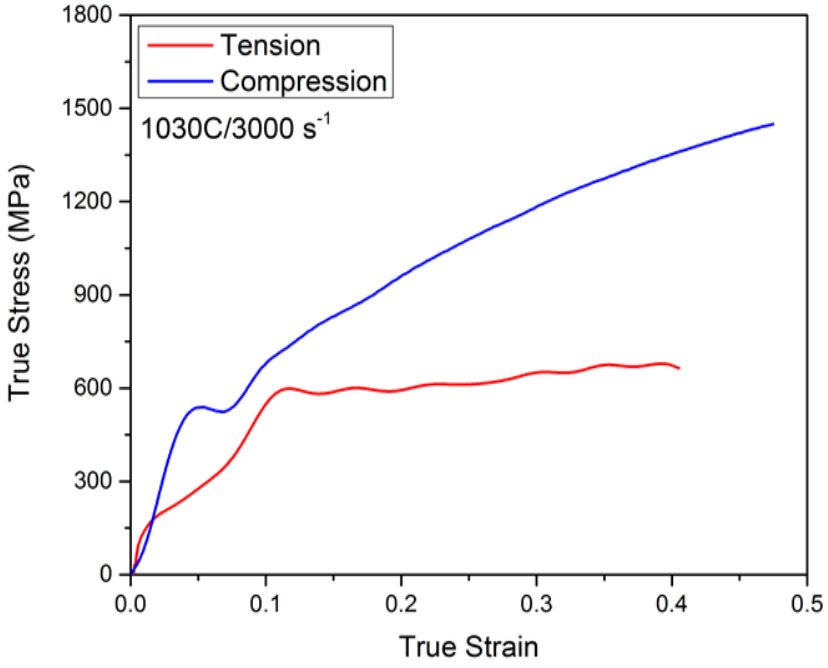

(d)

Figure 26. True tensile stress-strain curves. c) ~1030°C/1000 s^{-1}; d) ~1030°C/3000 s^{-1}

5. CONCLUSIONS

The conventional direct-tension Kolsky bar was modified for dynamic high-temperature tensile characterization of the DOP-26 iridium alloy. An induction coil was applied to heat the iridium specimen to elevated temperatures up to 1030°C while the specimen ends of the incident and transmission bars were cooled to reduce the thermal gradient in the bars. A pair of semiconductor strain gages on the transmission bar was used to directly measure the force/stress in the specimen during dynamic loading. A high-rate high-temperature DIC approach was conducted to evaluate the deformation uniformity in the specimen during dynamic loading. A laser system was developed to independently measure the displacements at the specimen ends on the incident- and transmission-bar sides such that the specimen strain could be calculated. A spring-loaded pretension system was installed on the free end of the transmission bar to prevent the high-temperature specimen from buckling during the heating process.

Dynamic tensile stress-strain curves of the iridium alloy were obtained at two elevated temperatures (750 and 1030°C) and strain rates (~1000 and 3000 s^{-1}). The iridium alloy possesses high ductility at elevated temperatures and strain rates. The effects of strain rate and temperature on the tensile stress-strain response of the iridium alloy were also determined. The iridium alloy exhibits little sensitivity to strain rate or temperature when the strain is below 10%, but strong sensitivities to both strain rate and temperature when the strain is greater than 10%.

Due to the high ductility of the DOP-26 iridium alloy at elevated temperatures, the tensile specimens did not fail during the first dynamic loading in most cases. However, the tensile specimens eventually failed after multiple dynamic loading cycles within a single dynamic test. The failure strains were estimated with the indentation marks on the surface of the specimen. The dynamic high-temperature tensile stress-strain curves of the DOP-26 iridium alloy were also compared with previous dynamic high-temperature compressive stress-strain data. Due to the different stress states of the specimens in dynamic tensile and compression tests, the flow stresses were higher in compression than in tension. The dynamic high-temperature stress-strain curves obtained in this study can be considered representative of the actual dynamic uniaxial stress-strain response of the DOP-26 iridium alloy.

This page intentionally left blank.

6. REFERENCES

1. Ohriner, E. K., *Processing of Iridium and Iridium Alloys, Methods from Purification to Fabrication,* Platinum Metals Review, 52:186-197 (1998).
2. Skrabek, E. A., *Consideration of Lower Allowable Impact Temperature for DOP26 Iridium Alloy Fueled Clads,* In: Proceedings of Space Technology and Applications International Forum – STAIF 2005, M. S. El-Genk (ed.), American Institute of Physics, pp. 776-781 (2005).
3. George, T. G., *High-strain-rate, High-temperature Biaxial Testing of DOP-26 Iridium,* Los Alamos National Laboratory Report, LA-11065, (1998).
4. Schneibel, J. H., Carmichael, C. A., George, E. P., *High Strain Rate Tensile Testing of DOP-26 Iridium,* Oak Ridge National Laboratory Report, ORNL/TM-2007/81 (2007).
5. George, E. P., Bei, H., Lee, E. H., Braden, J. D., *Tensile impact ductility and fracture behavior of DOP-26 iridium at 500-900°C,* Oak Ridge National Laboratory Report, ORNL/TM-2004/239.
6. McKamey, C. G., George, E. P., Lee, E. H., Ohriner, E. K., Cohron, J. W., *Impurity effects on high-temperature tensile ductility of iridium alloys at high strain rate*. Scripta Materials, 42:9-15 (2000).
7. Chen, W., Song, B., *Split Hopkinson (Kolsky) Bar, Design, Testing and Applications*, Springer New-York, (2011).
8. Song, B., Nelson, K., Lipinski, R., Bignell, J., Ulrich, G. B., George, E. P., *Dynamic High-temperature Characterization of an Iridium Alloy in Compression at High Strain Rates.* Sandia Report, SAND2014-15442 (2014).
9. Song, B., Nelson, K., Lipinski, R., Bignell, J., Ulrich, G., George, E. P., *Dynamic High-temperature Testing of an Iridium Alloy in Compression at High-strain Rates*. Strain, 50:539-546 (2014).
10. Kolsky, H., *An Investigation of the Mechanical Properties of Materials at Very High Rates of Loading*. Proceedings of Royal Society of London, B62:676-700 (1949).
11. Harding, J., Wood, E. O., Campbell, J. D., *Tensile Testing of Materials at Impact Rates of Strain*. Journal of Mechanical Engineering Science, 2:88-96 (1960).
12. Kawata, K., Hashimoto, S., Kurokawa, K., Kanayama, N., *A New Testing Method for the Characterization of Materials in High-Velocity Tension.* In: Mechanical Properties at High Rates of Strain, J. Harding (ed.), Institute of Physics Conference Series, 47:71-80 (1979).
13. Owens, A. T., Tippur, H. V., *Tensile Stress-Strain Response of Glass-Filled Epoxy under Elevated Rates of Loading Using a Split Hopkinson Bar Apparatus.* Experimental Mechanics, 49:799-811 (2009).
14. Song, B., Antoun, B. R., Connelly, K., Korellis, J., Lu, W.-Y., *Improved Kolsky Tension Bar for High-rate Tensile Characterization of Materials*. Measurement Science and Technology, 22:045704 (7pp).
15. Ramesh, K. T., Narasimhan, S., *Finite Deformations and the Dynamic Measurement of Radial Strains in Compression Kolsky Bar Experiments*. International Journal of Solids and Structures, 33:3723-3728 (1996).
16. Ostwaldt, D., Klepaczko, J. R., Klimanek, P., *Compression Tests of Polycrystalline α-iron up to high strains over a large range of strain rates*. Journal de Physique IV France, 7:385-390 (1997).

17. Li, Y., Ramesh, K. T., *An Optical Technique for Measurement of Material Properties in the Tension Kolsky Bar*. International Journal of Impact Engineering, 34:784-798.
18. Lim, J., Chen, W., Zheng, Q., *Dynamic Small Strain Measurements of Kevlar 129 Single Fibers with a Miniaturized Tension Kolsky Bar*. Polymer Testing, 29:701-705.
19. Hudspeth, M., Nie, X., Chen, W., Lewis, R., *Effect of Loading Rate on Mechanical Properties and Fracture Morphology of Spider Silk*. Biomacromodecules, 13:2240-2246 (2012).
20. Song, B., Antoun, B. R., Jin, H., *Dynamic Tensile Characterization of a 4330-V Steel with Kolsky Bar Techniques*. Experimental Mechanics, 53:1519-1529.
21. Barthelat, F., Wu, Z., Prorok, B. C., Espinosa, H. D., *Dynamic Torsion Testing of Nanocrystalline Coatings Using High-Speed Photography and Digital Image Correlation*. Experimental Mechanics, 43:331-340 (2003).
22. Mates, S. P., Rhorer, R., Everett, R. K., Simmonds, K. E., Bagchi, *A., High Strain Rate Tissue Simulant Measurement Using Digital Image Correlation.* In: Proceedings of the SEM 2009 Annual Conference, Albuquerque, NM, June 1-4, 2009.
23. Gilat, A., Schmidt, T. E., Walker, A. L., *Full Field Strain Measurement in Compression and Tensile Split Hopkinson Bar Experiments*. Experimental Mechanics, 49:291-302.
24. Su, J., Guo, W., Meng, W., Wang, J., *Plastic behavior and constitutive relations of DH-36 steel over a wide spectrum of strain rates and temperatures under tension*. Mechanics of Materials, 65:76-87 (2013).
25. Guo, W.-G., Gao, X., *On the constitutive modeling of a structural steel over a range of strain rates and temperatures,* Materials Science and Engineering, A561:468-476 (2013).
26. Feng, F., Huang, S., Meng, Z., Hu, J., Lei, Y., Zhou, M., Wu, D., Yang, Z., *Experimental study on tensils property of AZ31B magnesium alloy at different high strain rates and temperatures*, Materials and Design, 57:10-20 (2014).
27. Whittington, W. R., Oppedal, A. L., Turnage, S., Hammi, Y., Rhee, H., Allison, P. G., Crane, C. K., Horstemeyer, M. F., *Capturing the effect of temperature, strain rate, and stress state on the plasticity and fracture of rolled homogeneous armor (RHA) steel*, Materials Science and Engineering, A594:82-88 (2014).
28. Vilamosa, V., Clausen, A. H., Fagerholt, E., Hopperstad, O. S., Børvik, T., *Local measurement of stress-strain behaviour of ductile materials at elevated temperatures in a split-Hopkinson tension bar system*, Strain, 50:223-235 (2014).
29. Scapin, M., Peroni, L., Fichera, C., *Investigation of dynamic behaviour of copper at high temperature, Materials at High Temperatures*, 31:131-140 (2014).
30. Song, B., Lu, W.-Y., *Preload high-rate tension techniques,* In: Proceedings of SEM XII International Congress and Exposition on Experimental and Applied Mechanics, Costa Mesa, CA (2012).
31. Nie, X., Song, B., Loeffler, C. M., *A novel splitting-beam laser extensometer technique for Kolsky tension bar experiment*, Journal of Dynamic Behavior of Materials, 1:70-74 (2015).

DISTRIBUTION

1 US Department of Energy, NE-75
Office of Radioisotope Power Systems
Attn: Ryan D. Bechtel, (2)
19901 Germantown Road
Germantown, MD 20874

2 Tetra Tech, Inc.
Attn: Steven Giannino (2)
20251 Century Boulevard, Suite 200
Germantown, MD 20874-7114

1 Johns Hopkins University, 1E-255
Attn: Yale Chang (1)
Applied Physics Laboratory
11100 Johns Hopkins Road
Laurel, MD 20723

2 Oak Ridge National Laboratory
Attn: G. B. Ulrich (2)
P.O. Box 2008
Oak Ridge, TN 37831-6079

1 Ruhr University Bochum
Attn: E. P. George (1)
Institute for Materials
Faculty of Mechanical Engineering
Universitaetstr. 150
44801 Bochum, Germany

1	MS0557	D. Croessmann	Org. 1520
1	MS0557	D. Jones	Org. 1558
2	MS0557	B. Song	Org. 1558
1	MS0744	J. Bignell	Org. 6233
2	MS0747	R. Lipinski	Org. 6223
1	MS0815	J. Johannes	Org. 1500
1	MS0840	J. Redmond	Org. 1550
1	MS9014	C. Moen	Org. 8238
1	MS9042	J. Ostien	Org. 8256
1	MS9409	K. Nelson	Org. 8256
1	MS9957	H. Jin	Org. 8256
1	MS0899	Technical Library	9536 (electronic copy)

This page intentionally left blank.


Sandia National Laboratories